Chloride-binding capacity of hydrotalcite in cement pastes containing dolomite and metakaolin

Alisa Machner[1,2,*], Maciej Zajac[3], Mohsen Ben Haha[3], Knut O. Kjellsen[1], Mette R. Geiker[2], Klaartje De Weerdt[2]

[1]Norcem AS, R&D, Setreveien 2, P.O. Box 38, 3991 Brevik, Norway
[2]NTNU Department of Structural Engineering, Richard Birkelandsvei 1A, 7491 Trondheim, Norway
[3]Heidelberg Technology Center GmbH, Oberklamweg 2-4, 69181 Leimen, Germany

*Corresponding author: alisa.machner@ntnu.no
+47 45394622
ORCID-ID: 0000-0002-6334-5116

ABSTRACT

In this study, we investigated well-hydrated cement pastes containing dolomite and metakaolin cured at 38 °C or 60 °C, which were exposed to NaCl or $CaCl_2$ solutions of various concentrations. We determined the chloride-binding capacity, the phase assemblage and the composition of hydration phases formed. The dolomite reaction led to the formation of hydrotalcite, which contributed considerably to the chloride binding of the pastes. When the samples were exposed to $CaCl_2$, significantly more chlorides were bound in the hydrotalcite than when the samples were exposed to NaCl. It was shown that hydrotalcite contained a similar amount of chloride per mol compared to Friedel's salt when exposed to $CaCl_2$. By mass balance calculations, it was shown that the hydrotalcite formed in the samples containing dolomite can contribute to the chloride binding of the cement pastes to a similar extent as the Friedel's salt formed in the samples containing limestone.

Keywords:

EDX (B), Thermal Analysis (B), X-Ray Diffraction (B), Durability (C), Blended Cement (D)

1 INTRODUCTION

One of the main deterioration mechanisms for reinforced concrete structures is steel reinforcement corrosion. Reinforcement steel in sound concrete is passivated, i.e. does not corrode, due to the high pH of the concrete pore solution. However, in the presence of a sufficient level of chlorides, the steel is de-passivated and corrosion can occur. During the exposure to e.g. sea water or de-icing salts, chlorides ingress through the concrete cover towards the steel. Some chlorides will be free in the pore solution and some will interact with the hydrates in cement paste. In order to estimate the service life of reinforced concrete structures exposed to chlorides, we need to understand the interaction between concrete and chlorides.

Due to the increasing demand for cements and the need to reduce CO_2 emissions during production, new composite cements containing supplementary cementitious materials (SCMs) are being developed. In order to use these cements in reinforced concrete structures exposed to harsh environments such as marine exposure, there is a need to understand how these new binders interact with chlorides. In this study, we used dolomite and a combination of dolomite and metakaolin as SCMs to replace 40%wt of a Portland cement. We investigated the chloride-binding capacity of the hydrate phase assemblage for these new cements.

In an ordinary Portland cement, chloride ions have been reported to be physically adsorbed on the C-S-H phase or chemically bound by the formation of chloride-containing AFm phases, e.g. Friedel's salt ($3CaO{\cdot}Al_2O_3{\cdot}CaCl_2{\cdot}10H_2O$). The use of SCMs can change the phase assemblage of the hydrated cement paste and thereby its chloride-binding capacity [1].

The addition of metakaolin has been shown to improve the chloride-binding capacity of cement paste. This has been explained with reference to the additional alumina provided by the reaction of metakaolin, which results in the formation of additional Friedel's salt [2,3]. Similar results have been reported for other alumina-delivering SCMs, such as fly ash or ground granulated blast-furnace slags (GGBFS) [1,4–7]. Moreover, the reaction of metakaolin results in the formation of additional C-S-H, which may adsorb additional chlorides [8].

The addition of dolomite has been shown, depending on curing temperature, curing time, and metakaolin content, to result in the formation of significant amounts of a hydrotalcite-like phase (in the following referred to simply as hydrotalcite) [9,10]. Hydrotalcite is a mineral in the group of layered double hydroxides (LDHs) containing magnesium and aluminium, with the general formula $[Me^{2+}_{1-x}Me^{3+}_{x}(OH)_2]^{x+}\ [A^{m-}]_{x/m}{\cdot}nH_2O$. Its crystal structure can be derived from that of brucite. The main layer consists of metals (here abbreviated with Me), specifically magnesium

(Me^{2+}) and aluminium (Me^{3+}) hydroxide octahedra. The substitution of aluminium for magnesium in the main layer charges this layer positively. To maintain electrical neutrality, the interlayer incorporates monovalent or divalent anions (here abbreviated with A) , such as OH^-, Cl^-, CO_3^{2-} or SO_4^{2-}.

Several authors observed considerable chloride binding of hydrotalcite, either synthesized as a pure phase [11–13] or formed in GGBFS cement pastes [14,15]. We will investigate chloride binding of hydrotalcite originating from dolomite reaction in composite cements. In this system, the composition of the hydrotalcite differs from the before named studies both by the presence of carbonates or by the Mg/Al ratio of the hydrotalcite. Both factors influence the chloride-binding capacity of hydrotalcite.

Divalent ions, like CO_3^{2-} are more easily incorporated than monovalent ions, like Cl^- [11,12], so CO_3^{2-} ions are seldom exchanged with chloride ions in synthesized hydrotalcite-like phases, and the presence of carbonate ions consequently reduces the chloride-binding capacity [12,13].

A higher degree of aluminium substitution in the main layer, leading to a lower Mg/Al ratio of the hydrotalcite, increases the positive charge of the main layer. Because the interlayer seeks electrical neutrality, more anions, e.g. chlorides, are incorporated in the interlayer of hydrotalcite with a lower Mg/Al ratio [16]. The reduction of the Mg/Al ratio of the hydrotalcite can be caused by the presence of an aluminium-delivering SCM [10,17,18].

Moreover, it was reported that chlorides are also physically adsorbed on the surface of hydrotalcite adsorption [13,15].

The chloride-binding capacity of cements depends strongly on the cation associated with the chloride anion. Several authors have reported significantly greater chloride binding when samples were exposed to solutions of $CaCl_2$ or $MgCl_2$ rather than NaCl [1,3,19–23]. This difference has been largely attributed to the difference in the adsorption of chlorides onto the C-S-H and larger amount Friedel's salt. We will investigate whether the cation also influences the binding capacity of the hydrotalcite.

This study focuses on the impact of the hydrotalcite formed by the reaction of dolomite fines in the cement paste on the chloride binding of composite cement pastes. For this, cement paste samples in which 40%wt of the Portland cement was replaced by dolomite or by a combination of dolomite and metakaolin were investigated. Cement paste samples containing limestone instead of dolomite and a pure Portland cement sample were used as references. In order to be

able to study the effect of hydrotalcite, we needed samples containing sufficient amounts of hydrotalcite. Therefore, we investigates binder compositions containing dolomite and little or no metakaolin and cured at elevated temperatures, which according to an earlier study yielded considerable hydrotalcite formation [10]. Chloride-binding isotherms were experimentally obtained and related to the phase assemblage and phase composition of the solids obtained with XRD, TGA, and SEM-EDS. Additionally, the contribution of hydrotalcite, Friedel's salt, and C-S-H to the chloride binding of the cement pastes was evaluated using a mass balance approach.

2 EXPERIMENTAL

2.1 MATERIALS & SAMPLE PREPARATION

The materials used in this study were Portland cement (C) supplied by Norcem, to which gypsum but no limestone was added during grinding, natural dolomite (D), and natural limestone (L) supplied by Miljøkalk AS, and laboratory-grade metakaolin (M) supplied by Imerys (Metastar501). Table 1 shows the chemical composition, determined by X-ray fluorescence (XRF), of the materials used and their Blaine specific surface area. The particle size distributions of the materials used, determined by laser diffraction (Malvern Mastersizer 2000E), are shown in Figure 1. Table 2 gives an overview of the various sample compositions prepared. We replaced 40%wt of the Portland cement with either dolomite (60C40D) or a combination of 35%wt dolomite and 5%wt metakaolin (60C35D5M). The equivalent samples containing limestone (60C40L and 60C35L5M) and the Portland cement sample (100C) were used as references. Cement pastes were prepared with a w/b ratio of 0.5 for all binder compositions in a high-shear mixer (Braun MR5550CA). The mixing procedure was mixing for 30 s, resting for 5 min and mixing again for 60 s. The resting time of 5 min was chosen to check for false set of the paste. The resulting pastes were cast in 125 mL polyethylene screw-lid bottles, which were sealed with parafilm and stored, immersed up to their bottleneck, in water at 38 °C or 60 °C. After three months of curing, the hydrated cement pastes were removed from the bottles, crushed in a jaw-crusher and then ground in a rotating disc mill to a particle size <1 mm. The crushed cement paste was poured into 1 L screw-lid polypropylene bottles and 30%wt of deionized water relative to the crushed cement paste weight was added. The bottles were sealed with parafilm and cured for another four months at the respective temperatures. After a total of seven months of curing, the bottles were stored at 20 °C for two weeks before starting exposure at 20 °C. This sample preparation led to moist-sand like cement pastes. We chose this way of preparing the samples to maximize the degree of hydration of the binder before exposure and thus minimize any continued hydration during exposure.

2.2 CHLORIDE EXPOSURE

For the exposure, 30 g of the moist-sand-like cement paste was poured into 45 mL centrifuge tubes, to which 15 mL of exposure solution was added using a volumetric pipette. The exposure solutions were solutions of NaCl or $CaCl_2$ with chloride concentrations ranging from 0.25 to 3 mol/L, prepared with deionized water and laboratory-grade salts of NaCl or $CaCl_2 \cdot 2H_2O$ (supplied by Merck). The reference samples of all mixes were exposed to 15 mL of deionized water. The closed centrifuge tubes were shaken weekly and stored at 20 °C for at least one month to reach equilibrium prior to the investigation.

2.3 METHODS

2.3.1 Investigation of the supernatant

The chloride concentration in the supernatant was determined by potentiometric titration. The samples were centrifuged at 4000 rpm for 2.5 min. A known volume (0.2–0.8 mL, depending on the chloride concentration of the exposure solution) of the supernatant was pipetted into a measurement beaker, to which 1 mL of HNO_3 (65% supplied by Merck, and diluted 1:10), 2.5 mL of 0.2% polyvinyl alcohol (supplied by Merck, 2 g was dissolved in 1 L deionized water), and approx. 20 mL of deionized water were added. The chloride content was measured with a Titrando 905 titrator from Metrohm against a 0.1 mol/L $AgNO_3$ solution (Titrisol, supplied by Merck).

During the exposure of the cement paste, chlorides from the solution are taken up by the hydrates of the cement paste. The chloride concentration in the solution will therefore decrease. The amount of bound chlorides ($N_{Cl,bound}$) can be calculated as g/g cement paste using Eq. (1) [21].

$$N_{Cl,bound} = \frac{\left(C_{Cl,free} - C_{Cl,eq}\right) \cdot (V_{H_2O} + V_{Cl,added})/1000 \cdot M_{Cl}}{m_{sample} - m_{H_2O}} \quad (1)$$

where $C_{Cl,free}$ is the actual concentration of free chlorides present at the beginning of the exposure, which can be calculated using Eq. (2); $C_{Cl,eq}$ is the chloride concentration of the supernatant measured at equilibrium; V_{H2O} is the volume of free water in 30 g of the moist-sand-like hydrated cement paste before exposure; $V_{Cl,added}$ is the volume of exposure solution added (15 mL); M_{Cl} is the molar mass of chlorine (35.453 g/mol); m_{sample} is the mass of the sample added to the centrifuge tube (30 g); and m_{H2O} is the mass of free water in this 30 g of hydrated cement paste.

$$C_{Cl,free} = \frac{C_{Cl,added} \cdot V_{Cl,added}}{V_{H_2O} + V_{Cl,added}} \quad (2)$$

where $C_{Cl,added}$ is the concentration of chlorides in the exposure solution, which was measured with potentiometric titration prior to exposure. V_{H2O} was assumed to be equal to m_{H2O} and was determined by the weight loss of the moist-sand-like hydrated cement pastes after drying at 40 °C in a TGA until constant weight (Table 3).

A selection of samples was analysed in triplets. The average standard deviation obtained for the titrations of samples exposed to NaCl was approx. 10%. For samples exposed to $CaCl_2$, the average standard deviation of the titration experiments was approx. 5%. The standard deviations are indicated with by the error bars in the respective figures.

The experimental data obtained from the titration experiments with chloride concentrations from 0–3 mol/L were fitted with a Langmuir isotherm as shown in Eq. (3) [24].

$$N_{Cl,bound} = \frac{\alpha \cdot C_{Cl,free}}{(1 + \beta \cdot C_{Cl,free})} \quad (3)$$

where $N_{Cl,bound}$ are the amount of bound chlorides, $C_{Cl,free}$ the concentration of free chlorides before exposure, as described above, and α and β are fitting parameters, which depend on the binder composition [24].

After centrifuging, the pH of the supernatant was measured as well. This was done using a 6.0255.100 Profitrode from Metrohm. The measurements of the pH were performed in the laboratory at 20 °C. The electrode was calibrated on every measurement day with buffer solutions of pH 7, 10 and 13.

2.3.2 Investigation of the solids

The solid fraction was investigated on all samples exposed to a chloride concentration of 2 mol/L for NaCl and $CaCl_2$. The reference samples exposed to deionized water were also investigated. Approx. 6 g of the 30 g of each hydrated cement paste sample was taken out of the centrifuge tube after all the investigations of the liquids had been performed. To stop the hydration and remove the water or chloride solution, the wet hydrated cement paste was immersed in 100 mL isopropanol, shaken for 30 s, and left to rest for 5 min before the isopropanol was decanted. The isopropanol treatment was then repeated. After that, the sample was immersed in 20 mL petroleum ether, stirred for 30 sec, and left to rest again for 5 min. The petroleum ether was

filtrated off using a vacuum filtration unit, and the samples were dried in a desiccator overnight under a slight vacuum (-0.2 bar) applied using a water pump. The dried samples were ground to a particle size <63 µm and then analysed with TGA or XRD.

For the thermogravimetric analysis (TGA), approx. 150 mg of each ground sample was poured into a 600 µl corundum crucible. The weight loss was measured from 40–900 °C, with a heating rate of 10 °C/min in a Mettler Toledo TGA/DSC3+ device. During the experiments, the measurement cell was purged with 50 mL/min N_2 gas. TGA was used to identify changes in the phase assemblage and to quantify the amount of bound water and portlandite in each of the mixes investigated.

The derivate curves of the TG signal, the DTG curves, were used to detect phase changes. The DTG curves can be divided into several temperature intervals, in which the decomposition of specific phases can be detected as a weight loss. These temperature intervals were used to identify various hydration phases as suggested by Lothenbach et al. [25]. The first weight loss peak at around 100 °C is related to the ettringite (Et) decomposition and the beginning of the dehydroxylation of the C-S-H phase. C-S-H decomposes gradually between 40 °C and 600 °C and appears as a polynomial baseline under the other peaks. Hydrotalcite (Ht) shows two mass loss events, the first at approx. 220 °C and the second at around 400 °C. The subsequent sharp peak between approx. 400 °C and 550 °C is related to the decomposition of portlandite (CH). Above 550 °C, carbonates decompose by emitting CO_2. To make it possible to quantify the amount of bound water ($H_{dry\ binder\ weight}$) using Eq. (4) [26], the weight loss between 50 °C and approx. 550 °C was determined with a horizontal step. The weight loss related to the amount of portlandite was measured by integrating the DTG curve between approx. 400 °C and 550 °C with a linear baseline. This method is assumed to give similar results as using a tangential step and excludes the weight loss from the C-S-H decomposition still ongoing in this temperature region [25]. The portlandite content ($CH_{dry\ binder\ weight}$) can be calculated using Eq. (5) [26], where $M(Ca(OH)_2)$=74 g/mol and $M(H_2O)$=18 g/mol. Both quantifications in Eq. (4) and Eq. (5) are normalized to the dry binder weight, which is the sample weight at 550 °C and assumed to remain constant during hydration [26].

$$H_{dry\ binder\ weight} = \frac{w_{50} - w_{550}}{w_{550}} \tag{4}$$

$$CH_{dry\ binder\ weight} = \frac{w_{400} - w_{550}}{w_{550}} \cdot \frac{M(Ca(OH)_2)}{M(H_2O)} \tag{5}$$

The error for the $H_{dry\ binder\ weight}$ and $CH_{dry\ binder\ weight}$ is estimated to be 1% wt. The errors are indicated with the error bars in the respective figures.

To identify the gasses leaving the samples at a certain temperature interval, another TGA device (STA 449 C Jupiter from Netzsch) coupled with a quadrupole mass spectrometer unit (QMS 403 C Aëolos from Netzsch) was used. For these measurements, approx. 20 mg of selected samples were poured into corundum crucibles. The samples were analysed from 40–900 °C with a heating rate of 10 °C/min. During the measurement, the measurement cell was purged with 30 mL/min N_2 gas.

The X-ray diffraction (XRD) analyses were carried out using a D8 Focus from Bruker built with a Bragg-Brentano θ–2θ geometry, a LynxEye detector, and a goniometer radius of 200.5 mm. The samples were measured between 5 °2θ and 55 °2θ using Cu-Kα radiation with a wavelength of approx. 1.54 Å as X-ray source, a step size of 0.01 °2θ, and a sampling time per step of 0.5 s. The ground samples were front-loaded into the sample holders and queued in a sample changer until measurement (max. 4.5 h). The XRD plots were qualitatively evaluated using DIFFRAC.EVA V4.0 software from Bruker.

For the investigation of the hydrate phase assemblage with scanning electron microscopy (SEM), some of the hydration-stopped and dried but not ground samples were cast in epoxy, polished and carbon-coated. The investigated samples included all samples containing dolomite (60C40D and 60C35D5M) and the samples 60C35L5M exposed to NaCl or $CaCl_2$. Elemental mapping and point analyses were carried out using a Hitachi S-3400N electron microscope equipped with an energy dispersive spectrometer (EDS) from Oxford Instruments. The SEM was operated at an accelerating voltage of 15 keV, a working distance of 5 mm for taking the BSE images, and a working distance of 10 mm for operating the EDS. As reference samples, the results from a previous study [10] were used. In that study, the samples had similar binder compositions and were cured sealed at 100% RH for 360 days at 60 °C or 38 °C and prepared for SEM-EDS analysis in a similar way.

2.3.3 Thermodynamic modelling

The Gibbs free energy minimization program GEMS [27,28] was used to model the activity of CO_3^{2-} ions in the pore solution of a model system with increasing additions of NaCl or $CaCl_2$. The model system used consisted of 100 H_2O and 20 g $CaCO_3$. Because 0.03 g NaOH and 0.06 g KOH were included in the model, the pH at the starting point of the modelling was high (pH 13.9), which is similar to the pH in cementitious systems.

2.3.4 Mass balance calculations

The contribution of the various hydration phases to the chloride binding of the cement pastes was estimated with mass balance calculations for the samples 60C40D (60 °C) and 60C40L (38 °C) exposed to NaCl or $CaCl_2$. We used mass balance calculations instead of the thermodynamic

modelling software GEMS for this due to a lack of thermodynamic data for the chloride-containing hydrotalcite or the chloride uptake of the C-S-H. In a first step, the amount or volume of the various phases present in the system was calculated based on the following assumptions:

- For the cement, the QXRD results of a similar cement clinker and gypsum [10] were used as input for the calculations. The reaction degree of belite was set to 90% and the ferrite and periclase were assumed to not have reacted. All other components of the cement clinker and the gypsum were assumed to have reacted fully. For the dolomite ($CaMg(CO_3)_2$) a reaction degree of 30% was assumed when cured at 60 °C, and for the limestone ($CaCO_3$)a reaction degree of 5% was assumed when cured at 38 °C. The ideal stoichiometric compositions of dolomite and limestone were used as input for the calculations.
- The amount of calcium, aluminium, and sulphur in the C-S-H phase was calculated from the SEM-EDS point analysis results (Table 5), assuming 1 mol of C-S-H contains 1 mol of silicon.
- All the magnesium from the reaction of dolomite is bound in hydrotalcite. The hydrotalcite formula used for the calculations ($Mg_6Al_2(OH)_{18}{\cdot}3(H_2O)$) was taken from [29], because thermodynamic modelling of the reaction of dolomite in cement paste predicted the formation of a hydrotalcite, which does not contain carbonates [30], and the Mg/Al ratio of the hydrotalcite formed in the sample 60C40D was shown to be approx. 3 (Table 6).
- The amount of ettringite formed was calculated by subtracting the amount of sulphate in the C-S-H phase from the total amount of sulphates available in the system.
- The amount of AFm phases was calculated by subtracting the amount of aluminium incorporated in the C-S-H, ettringite, and hydrotalcite from the total amount of aluminium available in the system. The AFm phases taken into account for the calculations were monocarbonate and Friedel's salt. Several mass balance calculations were performed, in which the aluminium available for the formation of AFm phases was distributed in varying ratios to these two AFm phases (from 100% to 0% Friedel's salt and consequently 0% to 100% monocarbonate).
- The amount of secondary calcite, formed by the reaction of dolomite, was calculated by subtracting the amount of carbonates included in the monocarbonate from the total amount of carbonates available in the system.
- The amount of portlandite was calculated by the amount of calcium left in the system after subtracting the calcium incorporated in the C-S-H phase, secondary calcite, ettringite, monocarbonate, and Friedel's salt from the total amount of calcium available in the system.

Subsequently, the amount of chloride bound in the hydrotalcite, Friedel's salt, and C-S-H were calculated with the following steps:

- The amount of chloride in hydrotalcite[1] was calculated by the Mg/Al and Cl/Al ratio of the hydrotalcite determined with SEM-EDS (see Table 6).
- The amount of chloride in the Friedel's salt was calculated with its stoichiometric formula ($3CaO{\cdot}Al_2O_3{\cdot}CaCl_2{\cdot}10H_2O$), by taking into account the various amounts of Friedel's salt calculated, as described above.
- The amount of chloride in the C-S-H was determined by subtracting the amount of bound chlorides in hydrotalcite and Friedel's salt from the total amount of bound chlorides, as determined by potentiometric titration for the samples exposed to a 2 mol/L chloride solution (NaCl or $CaCl_2$) (see Figure 1). With this, the Cl/Si ratio of the C-S-H was calculated and compared to the Cl/Si ratio measured experimentally with SEM-EDS.

3 RESULTS

3.1 Chloride-binding isotherms

The results for the chloride-binding isotherms were plotted as the data points obtained experimentally by chloride titration and their corresponding fitted chloride-binding isotherms.

3.1.1 Chloride-binding isotherms of samples containing dolomite or limestone

Figure 2 shows the chloride-binding isotherms for samples 60C40D and 60C40L cured at 38 °C or 60 °C and exposed to NaCl. When cured at 38 °C, the sample containing limestone shows a similar chloride binding as the sample containing dolomite. However, when cured at 60 °C, the chloride binding of sample 60C40L drops slightly while sample 60C40D shows an increase.

3.1.2 Chloride-binding isotherms of samples containing a combination of dolomite or limestone with metakaolin

Figure 3 shows the chloride-binding isotherms for the samples cured at a) 38 °C and b) 60 °C exposed to NaCl. All samples cured at 38 °C and containing metakaolin, whether in combination with dolomite or limestone, showed a higher chloride binding than the 100C reference sample. Samples containing no metakaolin (60C40D and 60C40L) showed a lower chloride binding than the 100C reference. Moreover, the samples containing a combination of metakaolin and carbonate

[1]Due to the lack of an exact chemical formula for the chloride-containing hydrotalcite, we calculated its molar mass from the formula: $Mg_6Al_2(OH)_{18}{\cdot}3H_2O$.

(dolomite or limestone) did not seem to reach a plateau when they were exposed to chloride solutions with high concentrations, whereas the reference 100C and the samples 60C40D and 60C40L did.

When cured at 60 °C, the chloride binding of sample 60C40D was higher compared to 38 °C. Whereas for all other samples the chloride binding was lower at 60 °C compared to 38 °C. Sample 60C40D showed the highest chloride binding of the samples cured at 60 °C. Sample 60C35D5M showed a significantly lower chloride binding than sample 60C40D when cured at 60 °C.

3.1.3 Chloride-binding isotherms of samples exposed to $CaCl_2$

Figure 4 shows the chloride-binding isotherms for the samples exposed to various concentrations of $CaCl_2$ solution. The chloride-binding capacities were considerably higher for all samples exposed to $CaCl_2$ than for those exposed to NaCl (by a factor of 5–10).

Samples cured at 38 °C (Figure 4a) showed trends similar to those of the samples exposed to NaCl. Samples containing a combination of metakaolin and either dolomite or limestone showed a higher chloride binding than the 100C reference and gave the overall highest chloride binding of all samples investigated. Samples 60C40D and 60C40L showed a similar and low chloride binding.

For the samples cured at 60 °C (Figure 4b), however, the trends observed for the $CaCl_2$ exposure were different from those for NaCl. With $CaCl_2$ exposure, the samples containing dolomite, with or without metakaolin, showed very similar and the highest chloride binding of all samples cured at 60 °C. The reference sample 100C showed, as for NaCl exposure, a lower chloride binding than when cured at 38 °C. The samples containing limestone (60C40L, 60C35L5M) cured at 60 °C showed similar chloride binding and the lowest chloride binding of all the samples exposed to $CaCl_2$.

3.2 pH measurements

Figure 5 shows the results of the pH measurements of the supernatant of the various binder compositions cured at 38 °C and 60 °C and exposed to NaCl (Figure 5 a and b) and to $CaCl_2$ (Figure 5 c and d). The results of the pH measurements of the reference samples exposed to deionized water are plotted as the points for 0 mol/L added chloride concentration in all graphs.

All the samples containing SCMs that were exposed to NaCl showed a lower pH than the Portland cement sample 100C. This effect of SCMs on the pH of the pore solution has been described previously [31]. All samples containing SCMs and cured at 38 °C showed a very similar pH at all

concentrations of added chloride solution. The pH seemed to decrease only slightly with increasing chloride concentrations. The samples containing dolomite (60C40D and 60C35D5M) and cured at 60 °C, showed a lower pH than the samples containing limestone. This might be explained by the enhanced dolomite reaction at 60 °C, which has been shown to reduce the pH in a model system [32].

For $CaCl_2$ exposure, the 100C sample again showed a higher pH for all added chloride concentrations added than for the samples, in which 40%wt of the Portland cement was replaced with SCMs. The drop in the pH with increasing chloride concentrations was much greater than in the samples exposed to NaCl. This is attributed partly to the adsorption of calcium on silanol groups, which releases H^+-ions in the pore solution, and the common ion effect of portlandite (calcium hydroxide), as reported in the literature [3,20,22,23,33]. The decrease in the pH upon $CaCl_2$ addition results in a partial dissolution of the portlandite as experimentally observed in Figure 9.

There were no differences in the pH between the samples containing dolomite or limestone at either curing temperature when exposed to $CaCl_2$. This indicates that in the case of $CaCl_2$ exposure, the Ca^{2+} ions dominate the pH in contrast to the NaCl exposure, where the reaction of dolomite dominates the pH.

3.3 Thermodynamic modelling

Figure 6 shows the development of the activity of CO_3^{2-} ions in the solution and the amount of $CaCO_3$ present in the system with increasing additions of NaCl and $CaCl_2$ to the model system H_2O-$CaCO_3$ at a high pH. It can be seen that the activity of the carbonate ions is decreasing with increasing amounts of $CaCl_2$ added. First, the activity drops very rapidly and at free chloride concentrations higher than approx. 1.2 mol/L, the activity decreases with a smaller slope. The decrease in the carbonate ion activity is due to higher calcium concentration in the solution and the common ion effect, which is visible by the precipitation of small amounts of $CaCO_3$ in Figure 6. In the model system exposed to NaCl, however, there is no drop in the activity of carbonate ions within the range of the free chloride concentration modelled.

3.4 Hydrate phase assemblage of exposed samples determined with TGA and XRD

Table 4 gives a qualitative comparison of the phase assemblages observed with TGA or XRD in the various binder compositions cured at 38 °C or 60 °C and exposed to H_2O, NaCl or $CaCl_2$. In general, the results for TGA and XRD correlate well. In samples where we could only identify a phase with TGA but not with XRD, we assumed the phases to be poorly crystallized or amorphous. A detailed

description of the phase assemblages of the various samples and their associated TGA and XRD plots are given in the Appendix.

In the reference samples exposed to water, hydrotalcite formed in samples containing dolomite as detected with TGA and XRD. The weight loss peak of hydrotalcite increased with the curing temperature from 38 °C to 60 °C, for the samples containing dolomite. The samples containing limestone also showed a small weight loss in the temperature region of hydrotalcite. This weight loss in the samples could be associated with the decomposition of a siliceous hydrogarnet, because small peaks of this phase were observed with XRD in all the samples cured at 60 °C (not shown here). Monocarbonate was observed in all samples cured at 38 °C except 60C40D.

In samples exposed to NaCl or $CaCl_2$, chloride-containing phases were observed instead of monocarbonate or normal hydrotalcite. In samples containing dolomite, chloride-containing hydrotalcite, and in samples containing limestone, Friedel's salt was common. The chloride-containing hydrotalcite can be identified with XRD, as reported by Ke et al., by its the shift in the peak position to lower angles, as shown in Figure 7 [13]. Moreover, the signal in TGA also changed. The first peak of hydrotalcite (approx. 220 °C) decreased or completely disappeared and the second peak (approx. 400 °C) shifted to lower temperatures (approx. 370 °C) (Figure A1). The chloride-containing hydrotalcite was observed in chloride-exposed samples containing dolomite cured at both curing temperatures. A possible intermixing with Friedel's salt cannot be excluded, as the peaks of the chloride-containing hydrotalcite show a slightly asymmetric peak, which could indicate the presence of small amounts of Friedel's salt. Clear peaks of Friedel's salt were only visible in samples cured at 38 °C in the XRD and TGA graphs, though there was a small peak of Friedel's salt in sample 60C35L5M cured at 60 °C. In all samples exposed to $CaCl_2$, except sample 60C40D cured at 60 °C, a small hump of what was probably monosulphate-14H was observed. We could not identify this phase with TGA, probably due to its very small amounts and the overlapping of AFm decomposition peaks in the DTH curve. This indicates that the presence of calcium ions is also influencing the balance between monosulphate and ettringite, and not only the SO_3^{2-}/Al_2O_3 ratio of the pore solution. Sample 60C40D cured at 60 °C showed a monocarbonate peak instead of the monosulphate peak when exposed to $CaCl_2$.

It is important to note that, even though the TGA and XRD results correlate qualitatively very well, the ettringite peak in XRD seemed to be higher for the samples cured at 60 °C than for the samples cured at 38 °C. This increase was not observed with TGA. The reason for this is not clear, but it could be due to the sample preparation, in which the ettringite might have been severely

443 decomposed during the curing at 60 °C and re-crystallized later at 20 °C, potentially resulting in a
444 higher degree of crystallinity.
445
446 There were several peaks observed in the carbonate weight loss region of samples exposed to
447 either NaCl or $CaCl_2$. TGA-MS investigations of the sample 60C35D5M cured at 38 °C and exposed
448 to $CaCl_2$, showed that these peaks are related to the release of CO_2 (Figure 8). We expect the degree
449 of carbonation due to sample preparation to be similar in all samples, because they were all
450 prepared in the same way. The evaporation of chlorine, as reported for chloride-containing
451 hydrotalcite [13], is indicated by the increasing ion current for the chlorine (H-^{35}Cl, H-^{37}Cl, ^{35}Cl) at
452 temperatures >800 °C.
453
454 ## 3.5 Portlandite and bound water content
455
456 Figure 9 shows the portlandite content normalized to the dry binder weight of the various mixes
457 investigated. The portlandite content was lower in samples containing a combination of
458 metakaolin and carbonate (whether dolomite or limestone) than in samples containing only
459 carbonates as SCMs. Moreover, all samples containing dolomite and/or metakaolin showed a
460 lower portlandite content when cured at 60 °C than when cured at 38 °C. This can be explained by
461 the pozzolanic reaction of metakaolin to form additional C-S-H, and the reaction of dolomite to
462 form hydrotalcite and calcite, which both consume portlandite and are accelerated at elevated
463 curing temperatures. Only sample 60C40L exposed to $CaCl_2$ showed a higher portlandite content
464 when cured at 60 °C than when cured at 38 °C.
465
466 All samples exposed to chloride solutions showed a lower portlandite content than their reference
467 samples exposed to deionized water. This difference was greater for the exposure to $CaCl_2$ than to
468 NaCl. This was also experimentally observed in [22].
469
470 Figure 10 shows the amount of bound water in the various mixes investigated. The samples
471 containing dolomite or limestone show very similar results. The samples containing metakaolin
472 had a higher or similar bound water content compared to the 100C reference for both curing
473 temperatures. This indicates that the pozzolanic reaction of metakaolin, which forms additional
474 C-S-H and AFm phases, is able to compensate for the smaller amount of Portland cement in these
475 samples. The samples cured at 60 °C showed a lower bound water content than the samples cured
476 at 38 °C, even though, the clinker hydration and the pozzolanic reaction of metakaolin are
477 accelerated at elevated curing temperatures, and should thus lead to an increase in the bound
478 water content. The lower bound water content in samples cured at 60 °C compared to samples

cured at 38 °C might, however, be explained by the densification of the C-S-H at such high temperatures, which is associated with a loss of its structural water [34,35].

The bound water content changes for the various exposures. Samples exposed to NaCl showed a lower bound water content than their reference samples exposed to deionized water. Samples exposed to $CaCl_2$ showed a higher bound water content than samples exposed to NaCl, and in some cases a higher bound water content than samples exposed to deionized water.

Samples exposed to $CaCl_2$ show a lower portlandite and higher bound water content, than samples with the same composition exposed to NaCl. We, therefore, assume that the $CaCl_2$ reacted with the cementitious system to form additional phases. One possible reaction is the formation of calcium oxychloride phases from the reaction of $CaCl_2$ with water and portlandite [36–42]. However, we did not observe peaks of calcium oxychloride with XRD. This might be explained by the complexity of these salts, which were reported to decompose or carbonate easily during sample preparation [37,43].

3.6 Composition of the C-S-H and hydrotalcite in exposed samples measured with SEM-EDS

3.6.1 BSE imaging and elemental mapping

As an example of back-scattered electron (BSE) imaging, Figure 11 shows the BSE image and elemental maps of magnesium, aluminium, calcium, silicon and chlorine for sample 60C40D cured at 60 °C and exposed to NaCl. We chose this composition, because it showed the highest degree of dolomite reaction in a previous study [10]. The samples exposed to $CaCl_2$, as well as the samples 60C35D5M showed similar results. The up to 60 µm large uniformly grey particles are the unreacted parts of the dolomite particles. This is confirmed by the elemental maps, which show that these particles contain only magnesium and calcium. Around these particles, the original grain boundaries of the dolomite particles are still visible due to a thin layer of C-S-H that probably precipitated at early ages and persisted after the dolomite started to react. Between the original grain boundaries of dolomite and the boundary of the still unreacted dolomite particles, dark reaction rims are visible (highlighted with small arrows). These rims are rich in magnesium and aluminium but poor in calcium and silicon. Moreover, the rims seem to show a slightly higher chloride content than the matrix. The matrix shows a generally homogeneous chloride content. The small points of very high chlorine content in the last map are most probably crystals of NaCl that precipitated during drying in the samples. Point analyses of the samples exposed to NaCl or $CaCl_2$ were taken in the matrix of the samples and inside the reaction rims around the dolomite particles.

3.6.2 Effect of curing temperature, metakaolin addition and exposure solution on the composition of the C-S-H

Table 5 shows the results for the SEM-EDS point analyses of the matrix of selected samples exposed to NaCl or $CaCl_2$. The results given in Table 5 were determined by plotting the atomic ratios (e.g. Al/Ca over Si/Ca), in 2D diagrams. Tangents framing the C-S-H data cloud were used to discriminate the intermixed phases and determine the atomic ratios of the C-S-H phase.

The results for samples 60C40D exposed to NaCl show that the Si/Ca ratio and the Al/Si ratio of the C-S-H were lower in samples cured at 60 °C than in samples cured at 38 °C. This might be explained by the enhanced reaction of clinker and dolomite at 60 °C. Zajac et al. reported a lower aluminium content of the C-S-H in samples where dolomite reacted to hydrotalcite, which incorporates the aluminium instead [9].

In most of the samples containing metakaolin (60C35D5M and 60C35L5M) that were exposed to NaCl, the Al/Si and the Si/Ca ratio of the C-S-H is higher than in the samples containing no metakaolin (60C40D). This effect of the addition of metakaolin on the Si/Ca ratio of the C-S-H is qualitatively in agreement with literature [44,45]. However, it should be noted that the Si/Ca ratio of 0.9 for the sample 60C35L5M cured at 38 °C and exposed to NaCl is much higher than reported for the addition of 5%wt metakaolin [45]. The Si/Ca ratios of the other samples containing limestone and metakaolin are relatively similar. The reason for the high values for the sample 60C35L5M 38 °C NaCl are unclear. In samples exposed to $CaCl_2$, the Si/Ca ratio of the C-S-H was lower than in the samples exposed to NaCl for all samples except the sample 60C40D 38 °C.

To illustrate the chloride uptake of the C-S-H in these samples, Table 5 also shows the Cl/Si ratio of the point analyses of the matrix. For most of the samples, the Cl/Si ratio of the C-S-H is higher at 60 °C than at 38 °C. Exposure to $CaCl_2$ also increased the chloride content in the C-S-H compared to NaCl.

Table 5 also shows the S/Si ratio of the C-S-H in the various samples investigated. It can be seen that contradictive to the commonly observed higher sulphate content of C-S-H at higher curing temperatures, the S/Si ratio of the C-S-H in the samples cured at 60 °C was similar or lower than in the samples cured at 38 °C. This can be explained by the sample preparation, where the samples were cured at 60 °C or 38 °C, but exposed at 20 °C. This indicates that the C-S-H in the samples cured at 60 °C released a considerable amount of sulphate during the exposure at 20 °C, and can

explain the formation of ettringite or monosulphate in samples cured at 60 °C, as observed in with XRD.

3.6.3 Effect of metakaolin addition and exposure solution on the composition of hydrotalcite

The results for the point analyses taken in the reaction rims inside the original dolomite grains are shown in Figure 12 as the Mg/Ca ratio over the Al/Ca ratio. The results follow two linear lines, one for the hydrotalcite formed in samples containing dolomite (60C40D), and the other for the hydrotalcite formed in samples containing a combination of dolomite and metakaolin (60C35D5M). This indicates that no other aluminium-containing hydration products, such as Friedel's salt, were present in the reaction rims, as they would cause a spread of the result towards lower Mg/Al ratios. The different slopes of these lines indicate a decrease in the Mg/Al ratio of the hydrotalcite formed from approx. 3.2 in sample 60C40D to approx. 2.4 in sample 60C35D5M. The Mg/Al ratio does not seem to be affected by the exposure solution, but only by the presence of metakaolin.

Figure 13 shows the Cl/Ca over the Al/Ca ratio of the point analysis results in rims around the dolomite grains, which are filled with hydrotalcite. The slope of the lines indicated in Figure 13, presents the Cl/Al ratio of the hydrotalcite in the various samples, which is summarized for the various samples in Table 6. Hydrotalcite is reported to contain a constant amount of aluminium, but varying amounts of magnesium [46]. In this study we assumed hydrotalcite to always contain 2 mol of aluminium. Therefore, the results of the calculation of the amount of chloride ions in 1 mol of hydrotalcite show a lower chloride content in the hydrotalcite formed in samples containing metakaolin (Table 6).

3.7 Mass balance calculations

The amount of chloride bound in the C-S-H phase, Friedel's salt, and hydrotalcite per gram of cement paste in the samples 60C40D (60 °C) and 60C40L (38 °C) was calculated by a mass balance approach for exposure to either NaCl or $CaCl_2$. It is reported that with increasing concentrations of chlorides in the pore solution, monocarbonate transforms gradually to Friedel's salt [47]. With TGA and XRD it is not possible to distinguish Friedel's salt, hydrotalcite and monocarbonate completely. Especially, if little amounts of one of them are present in the samples. Due to the asymmetric peak of the chloride-containing hydrotalcite, the presence of Friedel's salt in samples containing dolomite cannot be excluded. Therefore, the aluminium available for the formation of AFm phases from the mass balance calculation was distributed in various ratios between monocarbonate and Friedel's salt (from 100% to 0% Friedel's salt and consequently 0% to 100%

monocarbonate). Figure 14 shows the amount of chloride bound in the various hydrates calculated by mass balance for the various combinations of monocarbonate and Friedel's salt.

For the high amounts of Friedel's salt assumed to be present, the calculated chloride content in the C-S-H phase shows negative values in case of exposure to NaCl. This is because the Cl/Si ratio of the C-S-H was calculated by subtracting the calculated amount of chloride bound in Friedel's salt and hydrotalcite from the total amount of chloride bound in the system measured. At high amounts of Friedel's salt present, more chlorides are calculated to be bound in the Friedel's salt than measured for the samples exposed to NaCl. We, therefore, assume these high Friedel's salt amounts to be an overestimation and concentrate in the following on the calculations where the aluminium available for the formation of AFm phases was distributed max. 30% to Friedel's salt (as indicated by the dashed rectangles). Because the hydrotalcite formed contains aluminium, less aluminium is available for the formation of AFm phases in the samples containing dolomite than in the sample containing limestone. This results in a smaller variation in the amount of chloride bound in the C-S-H or in the Friedel's salt in the sample 60C40D than in the sample 60C40L.

For the sample 60C40D, it was calculated that approx. 0.003 g of chlorides/g hydrated binder for NaCl exposure and approx. 0.006 g chlorides/g hydrated binder for $CaCl_2$ exposure were bound in hydrotalcite. For the sample 60C40L, where no hydrotalcite was formed, the maximum amount of chloride bound by Friedel's salt were approx. 0.003 g chlorides/g hydrated binder for NaCl exposure and approx. 0.002 g chlorides/g hydrated binder for $CaCl_2$ exposure.

We also used mass balance to calculate the Cl/Si ratio of the C-S-H, as described in 2.3.4. The highest Cl/Si ratios calculated for the C-S-H phase in sample 60C40D for NaCl or $CaCl_2$ exposure were approx. 0.03 and 0.15 respectively, which is considerably lower than the measured Cl/Si ratios of 0.1 and 0.24 for sample 60C40D cured at 60 °C (Table 5). This difference between measured and calculated Cl/Si ratios might be explained by the inability of the used solvents (isopropanol and petroleum ether) to penetrate the gel porosity of the C-S-H phase during the solvent exchange and replace the pore solution between the C-S-H sheets. This was explained by the big molecular size of alcohols compared to water, which inhibits the replacement of the water in very small pores [48]. Similarly, Plusquellec et al. showed that even methanol, which has a smaller molecular size than isopropanol, is unable to replace all the pore solution in ground concrete samples, leading to a lower amount of alkalis extracted from these samples [49]. In the present study, consequently, some of the chloride-rich solution would be trapped in the gel porosity and create an artificially high Cl/Si ratio in the point measurements with SEM-EDS.

Another possible explanation might be that the solubility of e.g. NaCl is much smaller in solvents than in water. Therefore, chloride salts, which might have precipitated in the sample during the solvent exchange, cannot be dissolved by the solvents.

The differences between the measured and calculated Cl/Si ratios of the C-S-H indicate that the solvent exchange treatment applied in this study is not a reliable method for sample preparation for SEM-EDS when the chloride content of the C-S-H needs to be measured. This is also indicated by the small points of very high chlorine content in the elemental map of chlorine (Figure 11), which are most probably crystals of NaCl that precipitated during the sample preparation.

The sample 60C40L was not investigated with SEM-EDS, and we can therefore not discuss on possible differences between the measured and calculated Cl/Si ratios in this samples.

We also calculated the portlandite content normalized to the dry binder weight of the samples 60C40D (60C40D-NaCl: 12 %wt, 60C40D-$CaCl_2$: 10 %wt) and 60C40L (60C40L-NaCl: 14 %wt, 60C40L-$CaCl_2$: 9 %wt) with the mass balance approach. We compared these values with the portlandite content normalized to the dry binder weight obtained experimentally with TGA (see Figure 9). Except for the sample 60C40L-$CaCl_2$, the portlandite content calculated with mass balance is larger than calculated with TGA. This indicates the formation of a calcium-containing phase in the samples exposed to the chloride solutions, which we did not account for in mass balance.

4 DISCUSSION

4.1 Chloride-binding isotherms for the samples containing limestone and metakaolin

The chloride binding of the samples containing limestone (60C40L and 60C35L5M) and the reference sample 100C was lower for the samples cured at 60 °C than of those cured at 38 °C (Figure 3 & Figure 4). This confirms the observations of other authors [50,51]. The increase in curing temperature from 38 °C to 60 °C changed the stability of some phases. This is visible in the XRD and TGA plots (results summarized in Table 4), where no or only small amounts of Friedel's salt can be observed with XRD and TGA in the samples cured at 60 °C. We, therefore, conclude that the lower chloride binding of samples containing limestone cured at 60 °C is due to the lower amount of chloride-containing hydrates in these samples.

When cured at 38 °C, where phases like Friedel's salt are observed with XRD and TGA, samples containing metakaolin show a higher chloride binding than samples without metakaolin (Figure 3a & Figure 4a). This effect has been explained by the additional aluminium delivered by the metakaolin [2,3]. The addition of aluminium enables the formation of more Friedel's salt and thereby increases the chloride-binding capacity of cement pastes. This is confirmed by our results, because we also observe an increase in the Friedel's salt with TGA in samples containing metakaolin (e.g. Figure A3).

4.2 Effect of hydrotalcite on the chloride binding in samples containing dolomite without metakaolin addition

Figure 2 shows the chloride-binding isotherms for the samples 60C40D and 60C40L cured at 38 °C, and 60 °C exposed to NaCl solutions. The sample 60C40D cured at 60 °C showed considerably greater chloride binding compared to the other samples. Assuming that the chloride content of the C-S-H is similar for the sample 60C40D and 60C40L, the increased chloride binding of the sample 60C40D cured at 60 °C will be due to the chloride binding in other hydrates than C-S-H. When cured at 60 °C, the dolomite in the samples has been shown to react significantly more than when cured at 38 °C and to form more hydrotalcite [9,10].

In the samples containing dolomite exposed to deionized water hydrotalcite formed, and in the samples exposed to a chloride solution a chloride-containing hydrotalcite was observed. This can be seen by the shift in the peak position of the hydrotalcite in XRD between the samples exposed to deionized water and those exposed to NaCl (Figure 7). A similar shift was observed previously by Ke et al. [13]. The peak position in XRD strongly depends on the c-parameter of the crystal lattice [52]. With the incorporation of chloride ions in the interlayer of the hydrotalcite the interlayer spacing is increased, because chloride ions have a larger ionic radius than hydroxide ions [11,13,16,53]. An increase in the c-parameter results in a lower angle for the diffraction peak of the phases. Moreover, the signal in TGA also changed, because the first peak of hydrotalcite (approx. 220 °C) decreased or completely disappeared and the second peak (approx. 400 °C) shifted to lower temperatures (approx. 370 °C) (Figure A1). Similar changes in the TGA signal upon the formation of a chloride-containing hydrotalcite were reported by Ke et al. [13]. However, the temperatures of these peaks in the present study vary from the temperatures reported by Ke et al. [13], probably because the hydrotalcite in this study was formed in a cementitious system rather than synthesised as a pure phase. The SEM-EDS point analyses (Figure 13) also showed a chloride uptake of the hydrotalcite in the samples exposed to NaCl. It should be noted that the amount of chloride in the hydrotalcite will be discussed in the following. Moreover, we do not observe clear peaks of Friedel's salt in sample 60C40D exposed to NaCl (Table 4). We, therefore,

conclude that the samples containing dolomite cured at 60 °C showed an increased chloride binding due to the formation of hydrotalcite, which is able to bind significant amounts of chloride. To which extent these chlorides are bound in the interlayer of the hydrotalcite or adsorbed on its surface could not be evaluated in with the experimental set-up in this study.

It should be noted that amongst the samples cured at 38 °C and exposed to NaCl, the reference sample 100C shows the highest chloride binding in the concentration range of a classic ponding test (0.5 mol/L). However, when cured at 60 °C, the sample 60C40D shows the highest chloride binding, also in this concentration range. As the curing at 60 °C was applied to accelerate the dolomite reaction, we assume the chloride binding of the sample 60C40D cured at 38 °C to increase with the increasing reaction degree of dolomite over time.

4.3 Effect of additional metakaolin on the composition and chloride-binding capacity of hydrotalcite

The Mg/Al ratio of hydrotalcite is known to be dependent on the availability of aluminium [17,18], and therefore on the addition of metakaolin [10]. The samples containing metakaolin cured at 60 °C showed a lower Mg/Al ratio of the hydrotalcite than in samples without metakaolin (Figure 12). The change in the Mg/Al ratio is also indirectly visible with XRD, where the hydrotalcite formed showed a peak at slightly higher angles in sample 60C35D5M than the sample 60C40D (Figure 7). This can be explained by the lower Mg/Al ratio of the hydrotalcite in the sample 60C35D5M, which increases the positive charge of the main layer [16]. Therefore, more anions are needed in the interlayer to compensate for the higher charge in the main layer, which reduced the c-parameter because of a shortening in the hydrogen bonds [54].

The calculations of the amount of chloride in 1 mol of hydrotalcite based on the SEM-EDS show a lower chloride content of the hydrotalcite in the samples 60C35D5M than in the samples 60C40D (Table 6). This is not in agreement with the literature, where it was reported that a lower Mg/Al ratio results in an increased uptake of chloride ions in the interlayer of hydrotalcite [16]. This was explained by the increased positive charge of the main layer due to aluminium having a higher charge than magnesium. Because the interlayer seeks electrical neutrality, more anions, in this case chlorides, should be taken up by the interlayer in the case of a decreased Mg/Al ratio [16]. The reason for the contradictive results in the present study are unknown.

The chloride-binding isotherms showed a lower chloride binding for the sample 60C35D5M cured at 60 °C and exposed to NaCl than for the sample 60C40D (Figure 3). Assuming that the apparent lower chloride-content of the hydrotalcite in the samples containing metakaolin is an artefact, one

728 possible explanation for this could be the lower amount of hydrotalcite in the sample 60C35D5M
729 compared to 60C40D. In a previous study, we showed that the amount of hydrotalcite formed
730 strongly depends on the availability of portlandite in the system, which decreased with the
731 amount of metakaolin added [10].
732
733 ## 4.4 Effect of the exposure solution on the chloride binding of the cement paste
734 ### 4.4.1 Effect of the exposure solution on the chloride-binding capacity of C-S-H
735 Samples exposed to $CaCl_2$ show a greater chloride binding than samples exposed to NaCl (Figure
736 3 and Figure 4). Several authors have described increased chloride binding when samples are
737 exposed to $CaCl_2$ rather than NaCl [1,3,19–23]. The difference might be due to the ability of
738 samples to accumulate chloride ions in the diffuse layer of the C-S-H in the case of $CaCl_2$ exposure
739 (Table 5). This has previously been explained by the overcompensation of the originally negative
740 surface charge of the C-S-H by the adsorption of divalent calcium ions in the Stern layer of the C-
741 S-H [55]. This overcompensation reverses the surface charge and turns it positive [55], which
742 means negatively charged chloride ions can accumulate in the diffuse layer of the C-S-H [8,23].
743 This is qualitatively in accordance with our results, as a higher Cl/Si ratio of the C-S-H phase was
744 measured in samples exposed to $CaCl_2$ compared to NaCl (see Table 5).
745
746 ### 4.4.2 Effect of the exposure solution on the chloride-binding capacity of
747 hydrotalcite
748 A higher chloride uptake in hydrotalcite was observed in the case of $CaCl_2$ exposure compared to
749 NaCl (Table 6). This could be explained using thermodynamic modelling, which showed that the
750 activity of the carbonate ions in the pore solution of a model system is decreased for $CaCl_2$
751 exposure, while it was not affected by NaCl exposure (Figure 6). Generally, divalent ions, such as
752 CO_3^{2-}, are more preferably incorporated in the interlayer of hydrotalcite than monovalent ions,
753 e.g. Cl^-. Due to the decrease of the activity of carbonate ions when exposed to $CaCl_2$, less carbonate
754 and more chloride ions might be accommodated in the interlayer of hydrotalcite in the case of
755 $CaCl_2$ exposure than in the case of NaCl exposure. The Mg/Al ratio of the hydrotalcite did not seem
756 to be affected by the exposure solution (Figure 12).
757
758 An additional explanation for the increased chloride uptake of hydrotalcite upon exposure to $CaCl_2$
759 compared to NaCl, is the decrease in the pH of the pore solution for $CaCl_2$ exposure, as shown in
760 Figure 5. Ke et al. highlighted the importance of the $[Cl^-]/[OH^-]$ ratio in the pore solution, which
761 can have a significant effect on the adsorption of chlorides on hydrotalcite. At a lower pH, the
762 concentration of OH^- ions is decreased, which might lead to the adsorption of chlorides rather than

763 hydroxides on the hydrotalcite [13]. In this study, we did however not differentiate between
764 surface adsorption and incorporation of chlorides in the interlayer of hydrotalcite.
765
766 **4.5 Comparison of the contribution of hydrotalcite and Friedel's salt to the**
767 **chloride binding of the cement pastes**
768 The amount of chloride bound in the C-S-H phase, Friedel's salt, and hydrotalcite per gram of
769 cement paste in the samples 60C40D (60 °C) and 60C40L (38 °C) exposed to either NaCl or $CaCl_2$
770 was calculated by a mass balance approach. The two different temperatures for the samples were
771 chosen, because considerable amounts of hydrotalcite were detected only in the samples
772 containing dolomite cured at 60 °C, whereas clear peaks of Friedel's salt were detected only in the
773 samples containing limestone cured at 38 °C.
774
775 The contribution of hydrotalcite, Friedel's salt and the C-S-H to the chloride binding of the cement
776 pastes exposed to a 2 mol/L chloride solution was estimated from the results of the mass balance
777 calculations shown in Figure 14. For the calculations where more than 30% of the aluminium
778 available for the formation of AFm phases is distributed to Friedel's salt, the Cl/Si ratio of the C-S-
779 H, and therefore its contribution to the chloride binding, is negative for the samples 60C40D and
780 60C40L exposed to NaCl, as described in 3.7. Negative values for the Cl/Si ratios are impossible,
781 and these calculations were not considered further. For the comparison between the contribution
782 of the chloride-containing hydrotalcite and the Friedel's salt to the chloride binding of the cement
783 paste, we chose the calculations were 25% of the aluminium is distributed to the formation of
784 Friedel's salt, as shown in Figure 15. This was done because the calculated Cl/Si ratio of the C-S-H
785 was similar between samples 60C40D an 60C40L in these calculations. The amount of chloride
786 bound in the hydrotalcite is unaffected by the combination of monocarbonate and Friedel's salt,
787 because the amount of hydrotalcite formed was assumed to depend solely on the reaction degree
788 of the dolomite.
789
790 The results of the mass balance calculations shown in Figure 15 indicate that the contribution of
791 hydrotalcite to the chloride binding of the sample 60C40D (60 °C) is in the range of Friedel's salt
792 in the sample 60C40L (38 °C) for both exposures.
793
794 However, the results of the mass balance calculations in this study are dependent on the amount
795 of hydrotalcite present, and therefore on the reaction degree of dolomite, which in this case is
796 assumed. Therefore, we also calculated the amount of chloride (N_{Cl}) in 1 mol of hydrotalcite (Table
797 6). We assumed hydrotalcite to contain always 2 mol of aluminium and varying amounts of
798 magnesium in the main layer. The Mg/Al and Cl/Al ratio of the hydrotalcite in sample 60C40D

were determined with SEM-EDS point analyses (Table 6). In case of NaCl exposure, 1 mol of the hydrotalcite formed contained approx. 0.8 moles of chlorides and in case of $CaCl_2$ exposure, approx. 1.8 mol of chlorides. For Friedel's salt, this value equals 2 according to its stoichiometric formula ($3CaO{\cdot}Al_2O_3{\cdot}CaCl_2{\cdot}10H_2O$). This indicates that the hydrotalcite formed due to the reaction of dolomite is able to bind similar amounts of chlorides compared to Friedel's salt when exposed to $CaCl_2$, and can, depending on the amount of hydrotalcite formed, contribute considerably to the chloride binding of the cement paste.

5 CONCLUSIONS

We investigated well-hydrated cement pastes in which 40%wt of the Portland cement was replaced with dolomite or a combination of dolomite and metakaolin cured at 38 °C or 60 °C. The pastes were exposed to NaCl, $CaCl_2$ or deionized water and the chloride binding, pH, phase assemblage and phase composition were determined. From the results the following conclusions can be drawn:

- The hydrotalcite that formed in samples containing dolomite contributed considerably to the chloride binding of these samples. This is especially visible in the samples containing dolomite cured at 60 °C, because higher curing temperatures resulted in an acceleration of the dolomite and reaction.
- In samples exposed to $CaCl_2$, hydrotalcite showed a higher chloride binding capacity than in samples exposed to NaCl. This can probably be explained by the decrease in the carbonate ion activity when the samples are exposed to $CaCl_2$, which might increase the uptake of chlorides instead of carbonates in the interlayer of hydrotalcite.
- With mass balance calculations, it was shown that the hydrotalcite in samples containing dolomite can contribute to the chloride binding of the cement pastes to a similar extent as the Friedel's salt formed in samples containing limestone.

6 Acknowledgements

The authors would like to thank the industrial PhD programme of the Norwegian Research Council (Project: 241637) and the Heidelberg Technology Center for their financial support. We are also grateful for the help and assistance of Tone Anita Østnor and Anne-Kristin Mjøen from SINTEF and the student assistants Petter Hemstad, Kristine Nøttveit, and Oda Tjeland from NTNU with the sample preparation and the chloride titration experiments.

7 References

[1] C. Arya, N.R. Buenfeld, J.B. Newman, Factors influencing chloride-binding in concrete, Cem Concr Res 20 (1990) 291–300.

[2] M.D.A. Thomas, R.D. Hooton, A. Scott, H. Zibara, The effect of supplementary cementitious materials on chloride binding in hardened cement paste, Cem Concr Res 42 (2012) 1–7.

[3] Z. Shi, M.R. Geiker, K. De Weerdt, T.A. Østnor, B. Lothenbach, F. Winnefeld, J. Skibsted, Role of calcium on chloride binding in hydrated Portland cement–metakaolin–limestone blends, Cem Concr Res 95 (2017) 205–216.

[4] C. Arya, Y. Xu, Effect of cement type on chloride binding and corrosion of steel in concrete, Cem Concr Res 25 (1995) 893–902.

[5] R.K. Dhir, M.A.K. El-Mohr, T.D. Dyer, Developing chloride resisting concrete using PFA, Cem Concr Res 27 (1997) 1633–1639.

[6] A. Ipavec, T. Vuk, R. Gabrovšek, V. Kaučič, Chloride binding into hydrated blended cements: The influence of limestone and alkalinity, Cem Concr Res 48 (2013) 74–85.

[7] O.R. Ogirigbo, L. Black, Chloride binding and diffusion in slag blends: Influence of slag composition and temperature, Constr Build Mater 149 (2017) 816–825.

[8] G. Plusquellec, A. Nonat, Interactions between calcium silicate hydrate (C-S-H) and calcium chloride, bromide and nitrate, Cem Concr Res 90 (2016) 89–96.

[9] M. Zajac, S.K. Bremseth, M. Whitehead, M. Ben Haha, Effect of $CaMg(CO_3)_2$ on hydrate assemblages and mechanical properties of hydrated cement pastes at 40 °C and 60 °C, Cem Concr Res 65 (2014) 21–29.

[10] A. Machner, M. Zajac, M. Ben Haha, K.O. Kjellsen, M.R. Geiker, K. De Weerdt, Limitations of the hydrotalcite formation in Portland composite cement pastes containing dolomite and metakaolin, Manuscript submitted for publication (2017).

[11] S. Miyata, Anion-Exchange Properties of Hydrotalcite-Like Compounds, Clays and Clay Minerals 31 (1983) 305–311.

[12] L. Châtelet, J.Y. Bottero, J. Yvon, A. Bouchelaghem, Competition between monovalent and divalent anions for calcined and uncalcined hydrotalcite: anion exchange and adsorption sites, Colloids and Surfaces A 111 (1996) 167–175.

[13] X. Ke, S.A. Bernal, J.L. Provis, Uptake of chloride and carbonate by Mg-Al and Ca-Al layered double hydroxides in simulated pore solutions of alkali-activated slag cement, Cem Concr Res 100 (2017) 1–13.

[14] O. Kayali, M.S.H. Khan, M. Sharfuddin Ahmed, The role of hydrotalcite in chloride binding and corrosion protection in concretes with ground granulated blast furnace slag, Cement and Concrete Composites 34 (2012) 936–945.

[15] H. Ye, X. Jin, W. Chen, C. Fu, N. Jin, Prediction of chloride binding isotherms for blended cements, Computers and Concrete 17 (2016) 655–672.
[16] S. Miyata, The Syntheses of Hydrotalcite-Like Compounds and Their Structures and Physico-Chemical Properties I: The Systems Mg^{2+}-Al^{3+}-NO_3^-, Mg^{2+}-Al^{3+}-Cl^-, Mg^{2+}-Al^{3+}-ClO_4^-, Ni^{2+}-Al^{3+}-Cl^- and Zn^{2+}-Al^{3+}-Cl^-, Clays and Clay Minerals 23 (1975) 369–375.
[17] R. Taylor, I.G. Richardson, R.M.D. Brydson, Composition and microstructure of 20-year-old ordinary Portland cement–ground granulated blast-furnace slag blends containing 0 to 100% slag, Cem Concr Res 40 (2010) 971–983.
[18] M. Ben Haha, B. Lothenbach, G. Le Saout, F. Winnefeld, Influence of slag chemistry on the hydration of alkali-activated blast-furnace slag – Part II: Effect of Al_2O_3, Cem Concr Res 42 (2012) 74–83.
[19] A. Delagrave, J. Marchand, J.-P. Ollivier, S. Julien, K. Hazrati, Chloride Binding Capacity of Various Hydrated Cement Paste Systems, Advanced Cement Based Materials 6 (1997) 28–35.
[20] Q. Zhu, L. Jiang, Y. Chen, J. Xu, L. Mo, Effect of chloride salt type on chloride binding behavior of concrete, Construction and Building Materials 37 (2012) 512–517.
[21] K. De Weerdt, D. Orsáková, M.R. Geiker, The impact of sulphate and magnesium on chloride binding in Portland cement paste, Cem Concr Res 65 (2014) 30–40.
[22] K. De Weerdt, A. Colombo, L. Coppola, H. Justnes, M.R. Geiker, Impact of the associated cation on chloride binding of Portland cement paste, Cem Concr Res 68 (2015) 196–202.
[23] O. Wowra, M.J. Setzer, Sorption of chlorides on hydrated cement and C_3S pastes, in: M.J. Setzer, R. Auberg (Eds.), Frost Resistance of Concrete, E & FN Spon, London, 1997, pp. 147–153.
[24] Q. Yuan, C. Shi, G. de Schutter, K. Audenaert, D. Deng, Chloride binding of cement-based materials subjected to external chloride environment – A review, Constr Build Mater 23 (2009) 1–13.
[25] B. Lothenbach, P. Durdzinski, K. De Weerdt, Thermogravimetric Analysis, in: K.L. Scrivener, R. Snellings, B. Lothenbach (Eds.), A Practical Guide to Microstructural Analysis of Cementitious Materials, CRC Press Taylor & Francis Group, Boca Raton, 2015, pp. 177–211.
[26] K. De Weerdt, E. Sellevold, K.O. Kjellsen, H. Justnes, Fly ash–limestone ternary cements: effect of component fineness, Advances in Cement Research 23 (2011) 203–214.
[27] D. Kulik, GEM-Selektor v.3.3, available at: http://gems.web.psi.ch/.
[28] B. Lothenbach, F. Winnefeld, Thermodynamic modelling of the hydration of Portland cement, Cem Concr Res 36 (2006) 209–226.
[29] R.J. Myers, B. Lothenbach, S.A. Bernal, J.L. Provis, Thermodynamic modelling of alkali-activated slag cements, Applied Geochemistry 61 (2015) 233–247.

[30] A. Machner, M. Zajac, M. Ben Haha, K.O. Kjellsen, M.R. Geiker, K. De Weerdt, Portland metakaolin cement containing dolomite or limestone – Similarities and differences in phase assemblage and compressive strength, Constr Build Mater 157 (2017) 214–225.
[31] B. Lothenbach, K.L. Scrivener, R.D. Hooton, Supplementary cementitious materials, Cem Concr Res 41 (2011) 1244–1256.
[32] E. Garcia, P. Alfonso, M. Labrador, S. Galí, Dedolomitization in different alkaline media: Application to Portland cement paste., Cem Concr Res 33 (2003) 1443–1448.
[33] J. Tritthart, Chloride binding in cement - II. The influence of the hydroxide concentration in the pore solution of hardened cement paste on chloride binding, Cem Concr Res 19 (1989) 683–691.
[34] B. Lothenbach, F. Winnefeld, C. Alder, E. Wieland, P. Lunk, Effect of temperature on the pore solution, microstructure and hydration products of Portland cement pastes, Cem Concr Res 37 (2007) 483–491.
[35] E. Gallucci, X. Zhang, K.L. Scrivener, Effect of temperature on the microstructure of calcium silicate hydrate (C-S-H), Cem Concr Res 53 (2013) 185–195.
[36] L. Berntsson, S. Chandra, Damage of concrete sleepers by calcium chloride, Cement and Concrete Research 12 (1982) 87–92.
[37] K. Peterson, G. Julio-Betancourt, L. Sutter, R.D. Hooton, D. Johnston, Observations of chloride ingress and calcium oxychloride formation in laboratory concrete and mortar at 5°C, Cement and Concrete Research 45 (2013) 79–90.
[38] L. Sutter, K. Peterson, S. Touton, T. van Dam, D. Johnston, Petrographic evidence of calcium oxychloride formation in mortars exposed to magnesium chloride solution, Cement and Concrete Research 36 (2006) 1533–1541.
[39] H.G. Smolczyk, Chemical reactions of strong chloride-solutions with concrete, in: S. Kyōkai (Ed.), Proceedings of the 5th International Symposium on the Chemistry of Cement, 1968.
[40] M. Collepardi, L. Coppola, C. Pistolesi, Durability of concrete structures exposed to $CaCl_2$ based de-icing salts, in: V.M. Malhotra (Ed.), Proceedings of the third CANMET/ACI International Conference of Durability of Concrete, American Concrete Institute, 1994.
[41] H. Justnes, K. De Weerdt, M.R. Geiker, Chloride binding in concrete exposed to sea water and salt solutions, in: Z.J. Li, C.W. Miao, O.E. Gjørv, W. Sun, K. Sakai, N. Banthia (Eds.), Seventh International Conference on Concrete under Severe Conditions (CONSEC13) Nanjing, China, 23-25 September 2013, RILEM proceedings PRO, 2013, pp. 647–659.
[42] G. Julio-Betancourt, Effect of de-icer and anti-icer chemicals on the durability, microstructure, and properties of cement-based materials. Ph.D. Thesis, University of Toronto, 2009.

[43] C. Shi, Formation and stability of $3CaO{\cdot}CaCl_2{\cdot}12H_2O$, Cement and Concrete Research 31 (2001) 1373–1375.
[44] Z. Dai, T.T. Tran, J. Skibsted, H. Jennings, Aluminum Incorporation in the C-S-H Phase of White Portland Cement-Metakaolin Blends Studied by ^{27}Al and ^{29}Si MAS NMR Spectroscopy, J. Am. Ceram. Soc. 97 (2014) 2662–2671.
[45] W. Kunther, Z. Dai, J. Skibsted, Thermodynamic modeling of hydrated white Portland cement–metakaolin–limestone blends utilizing hydration kinetics from ^{29}Si MAS NMR spectroscopy, Cem Concr Res 86 (2016) 29–41.
[46] K. Morimoto, S. Anraku, J. Hoshino, T. Yoneda, T. Sato, Surface complexation reactions of inorganic anions on hydrotalcite-like compounds, Journal of Colloid and Interface Science 384 (2012) 99–104.
[47] M. Balonis, B. Lothenbach, G. Le Saout, F.P. Glasser, Impact of chloride on the mineralogy of hydrated Portland cement systems, Cem Concr Res 40 (2010) 1009–1022.
[48] J. Zhang, G.W. Scherer, Comparison of methods for arresting hydration of cement, Cem Concr Res 41 (2011) 1024–1036.
[49] G. Plusquellec, M.R. Geiker, J. Lindgård, J. Duchesne, B. Fournier, K. De Weerdt, Determination of the pH and the free alkali metal content in the pore solution of concrete: Review and experimental comparison, Cement and Concrete Research 96 (2017) 13–26.
[50] M.H. Roberts, Effect of calcium chloride on the durability of pre-tensioned wire in prestressed concrete, Magazine of Concrete Research 14 (1962) 143–154.
[51] S.E. Hussain, Rasheeduzzafar, Effect of temperature on pore solution composition in plain cements, Cem Concr Res 23 (1993) 1357–1368.
[52] T. Witzke, L. Torres-Dorante, F. Bullerjahn, H. Pöllmann, Use of Layered Double Hydroxides (LDH) of the Hydrotalcite Group as Reservoir Minerals for Nitrate in Soils – Examination of the Chemical and Mechanical Stability, in: S.V. Krivovichev (Ed.), Minerals as Advanced Materials II, Springer Berlin Heidelberg, Berlin, Heidelberg, 2012, pp. 131–145.
[53] A. de Roy, Lamellar Double Hydroxides, Molecular Crystals and Liquid Crystals Science and Technology. Section A. Molecular Crystals and Liquid Crystals 311 (1998) 173–193.
[54] G. Mascolo, O. Marino, A new synthesis and characterization of magnesium-aluminium hydroxides, Mineral. Mag. 43 (1980) 619–621.
[55] C. Labbez, A. Nonat, I. Pochard, B. Jönsson, Experimental and theoretical evidence of overcharging of calcium silicate hydrate, Journal of Colloid and Interface Science 309 (2007) 303–307.

Tables

Table 1: Chemical composition of the Portland cement, dolomite, limestone and metakaolin used, as determined by XRF [%wt] and their Blaine surface areas [m^2/kg].

Oxide	Portland cement	Dolomite	Limestone	Metakaolin
SiO_2	19.91	0.52	0.12	52.18
Al_2O_3	5.15	0.01	0.06	44.92
TiO_2	0.282	0.00	0.00	1.14
MnO	0.062	0.00	0.00	0.00
Fe_2O_3	3.42	0.04	0.03	0.62
CaO	62.73	31.52	55.12	0.12
MgO	2.34	20.14	0.41	0.04
K_2O	1.09	0.00	0.01	0.18
Na_2O	0.48	0.00	0.00	0.17
SO_3	3.16	0.00	0.02	0.14
P_2O_5	0.109	0.01	0.00	0.07
LOI	1.07	46.79	43.57	0.29
Sum (1050 °C)	**99.80**	**99.03**	**99.34**	**99.87**
Blaine [m^2/kg]	**416**	**340**	**370**	**987**

Table 2: Matrix for the mixes [%wt]. The sulphate content of the Portland cement was set to 3.2%wt.

Name	C Portland cement	D Dolomite	L Limestone	M Metakaolin
100C	100	-	-	-
60C40D	60	40	-	-
60C35D5M	60	35	-	5
60C40L	60	-	40	-
60C35L5M	60	-	35	5

Table 3: Overview of the weight losses of the various well-hydrated samples before exposure during drying at 40 °C until constant weight [%wt]. The accuracy was estimated to 1%wt.

Sample name	Curing temperature [°C]	Weight loss drying at 40 °C [%wt]
100C	38 °C	33
60C40D	38 °C	35
60C35D5M	38 °C	35
60C40L	38 °C	39
60C35L5M	38 °C	37
100C	60 °C	32
60C40D	60 °C	35
60C35D5M	60 °C	35
60C40L	60 °C	37
60C35L5M	60 °C	38

Table 4: Phase assemblage of ettringite (Et), monosulphate-14H (Ms), monocarbonate (Mc), Friedel's salt (Fs), chloride-containing hydrotalcite (Ht_{Cl}), and hydrotalcite (Ht) observed with TGA or XRD in the various mixes for various curing temperatures (38 °C, 60 °C) and exposures (H_2O, NaCl, $CaCl_2$). The text in brackets indicates a low signal of that phase or an overlap with another peak so that its presence could not be confirmed nor excluded.

Sample	Exposure	Temp.	Et	Ms-14	Mc	Fs	Ht_{Cl}	Ht
60C40D	H_2O	38 °C	TGA|XRD					TGA|XRD
		60 °C						TGA|XRD
60C35D5M	H_2O	38 °C	TGA|XRD		TGA|XRD			TGA|(XRD)
		60 °C	(TGA)|XRD					TGA|XRD
60C40L	H_2O	38 °C	TGA|XRD		TGA|XRD			(TGA)
		60 °C	TGA|XRD					(TGA)
60C35L5M	H_2O	38 °C	TGA|XRD		TGA|XRD			(TGA)
		60 °C	TGA|XRD					(TGA)
60C40D	NaCl	38 °C	TGA			(XRD)	TGA|XRD	
		60 °C				(XRD)	TGA|XRD	
60C35D5M	NaCl	38 °C	TGA		(TGA)	(TGA)|XRD	TGA|(XRD)	
		60 °C	(TGA)|XRD			(XRD)	TGA|XRD	(TGA)
60C40L	NaCl	38 °C	TGA		(TGA)	TGA|XRD	(TGA)	
		60 °C	TGA|XRD			(TGA)	(TGA)	
60C35L5M	NaCl	38 °C	TGA		TGA	TGA|XRD	(TGA)	
		60 °C	(TGA)			(TGA)|XRD	(TGA)	
60C40D	$CaCl_2$	38 °C	TGA	(XRD)		TGA|(XRD)	TGA|XRD	
		60 °C			TGA|XRD	(XRD)	TGA|XRD	
60C35D5M	$CaCl_2$	38 °C	TGA	(XRD)		TGA|XRD	TGA	
		60 °C	TGA	(XRD)		(XRD)	TGA|XRD	
60C40L	$CaCl_2$	38 °C	TGA	(XRD)		TGA|XRD	(TGA)	
		60 °C	TGA|XRD	(XRD)			(TGA)	
60C35L5M	$CaCl_2$	38 °C	TGA	(XRD)		TGA|XRD	(TGA)	
		60 °C	TGA	(XRD)		TGA|XRD	(TGA)	

Table 5: Overview of the C-S-H composition of the samples 60C40D, 60C35D5M, and 60C35L5M cured at 38 °C or 60 °C and exposed to NaCl or $CaCl_2$.

Sample			Si/Ca	Al/Si	Cl/Si	S/Si
60C40D	38 °	NaCl	0.68	0.03	0.05	0.03
		$CaCl_2$	0.78	0.04	0.24	0.03
	60 °	NaCl	0.58	0	0.1	0.04
		$CaCl_2$	0.55	0	0.24	0.04
60C35D5M	38 °	NaCl	0.78	0.04	0.05	0.04
		$CaCl_2$	0.75	0.06	0.19	0.03
	60 °	NaCl	0.73	0.04	0.16	0.02
		$CaCl_2$	0.65	0.04	0.24	0.02
60C35L5M	38 °	NaCl	0.9	0.08	0.05	0.04
		$CaCl_2$	0.65	0.08	0.2	0.03
	60 °	NaCl	0.65	0.04	0.16	0.008
		$CaCl_2$	0.56	0.04	0.24	0.008

Table 6: Overview of the Mg/Al and Cl/Al ratio of the hydrotalcite in the various samples, and the amount of chloride calculated [mol] per 1 mol of hydrotalcite (N_{Cl}).

Sample			Mg/Al	Cl/Al	N_{Cl}
Hydrotalcite	60C40D	NaCl	3.2	0.4	0.8
		$CaCl_2$	3.2	0.9	1.8
	60C35D5M	NaCl	2.4	0.2	0.4
		$CaCl_2$	2.4	0.7	1.4

996 **Figures**

997

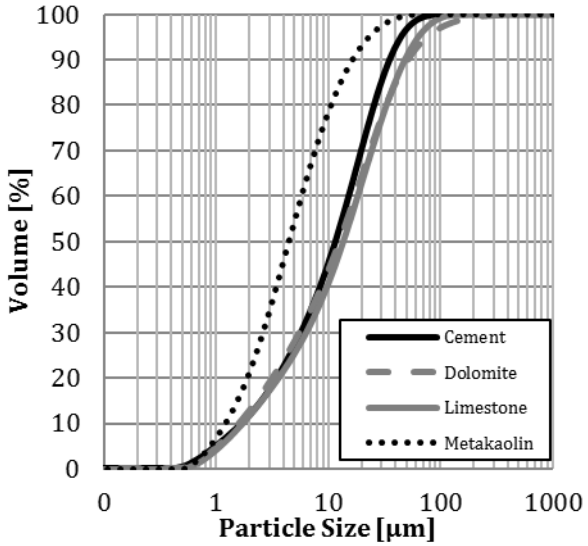

Figure 1: Particle size distribution of the materials used determined by laser diffraction.

998

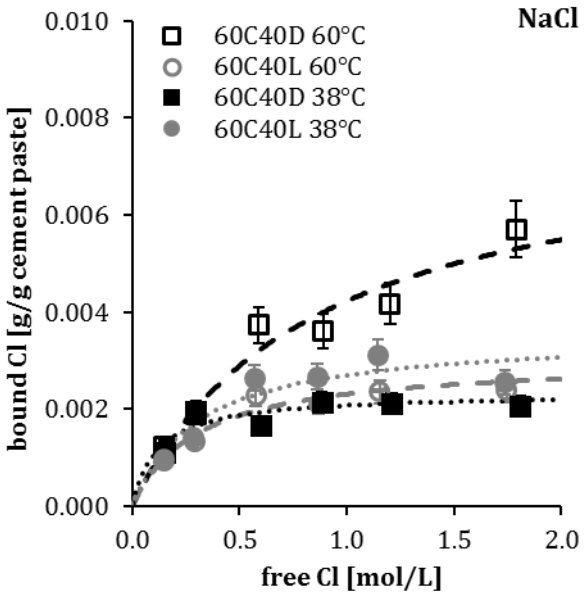

Figure 2: Experimental data and fitted curves of the chloride-binding isotherms for the samples 60C40D (*black squares*) and 60C40L (*grey spheres*) cured at 38 °C (*filled icons, dotted lines*) or 60 °C (*hollow icons, dashed lines*) and exposed to NaCl.

999

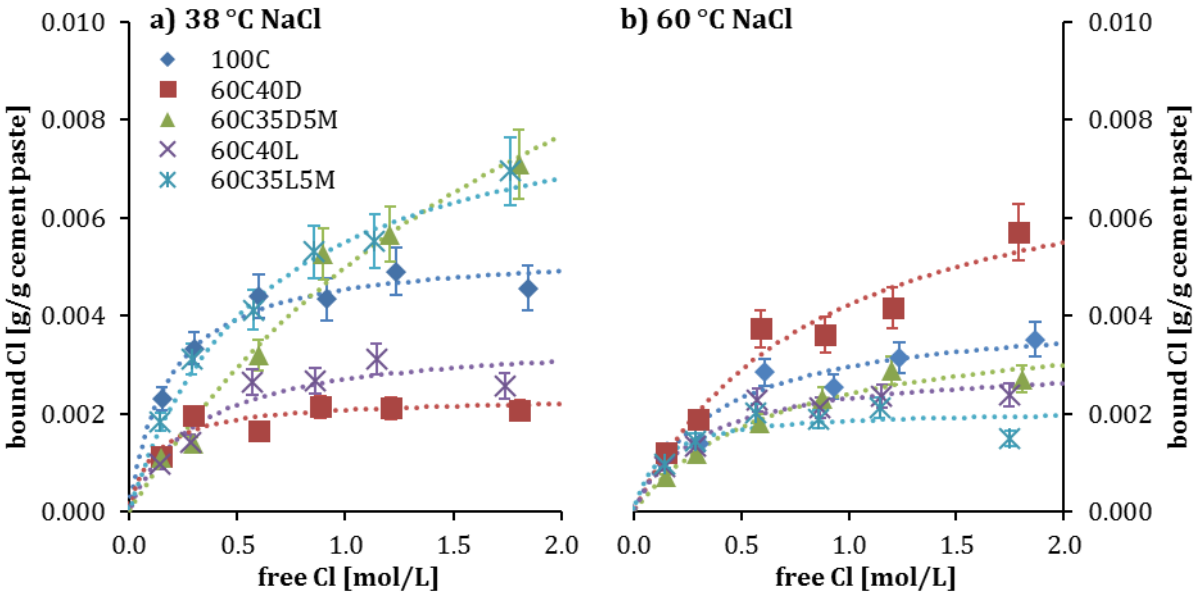

Figure 3: Experimental data and fitted curves of the chloride-binding isotherms for all the mixes investigated that were cured at a) 38 °C or b) 60 °C and exposed to NaCl.

1000

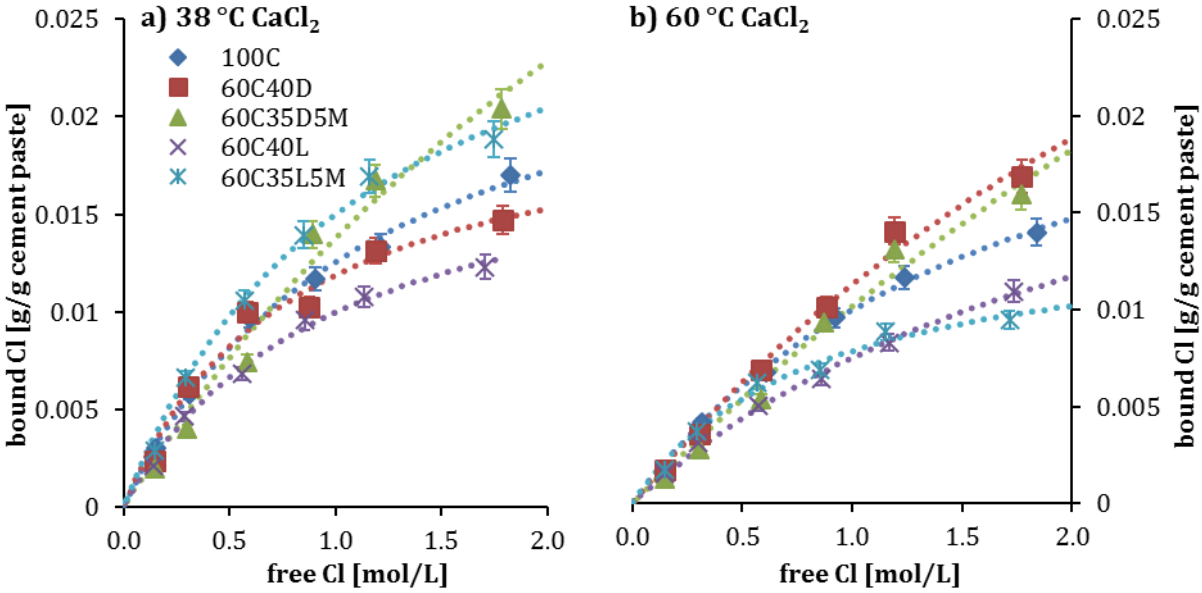

Figure 4: Experimental data and fitted curves of the chloride-binding isotherms for all the mixes investigated that were cured at a) 38 °C or b) 60 °C and exposed to $CaCl_2$. Note that the scale of the y-axis is different compared to Figure 2 and Figure 3.

1001

1002

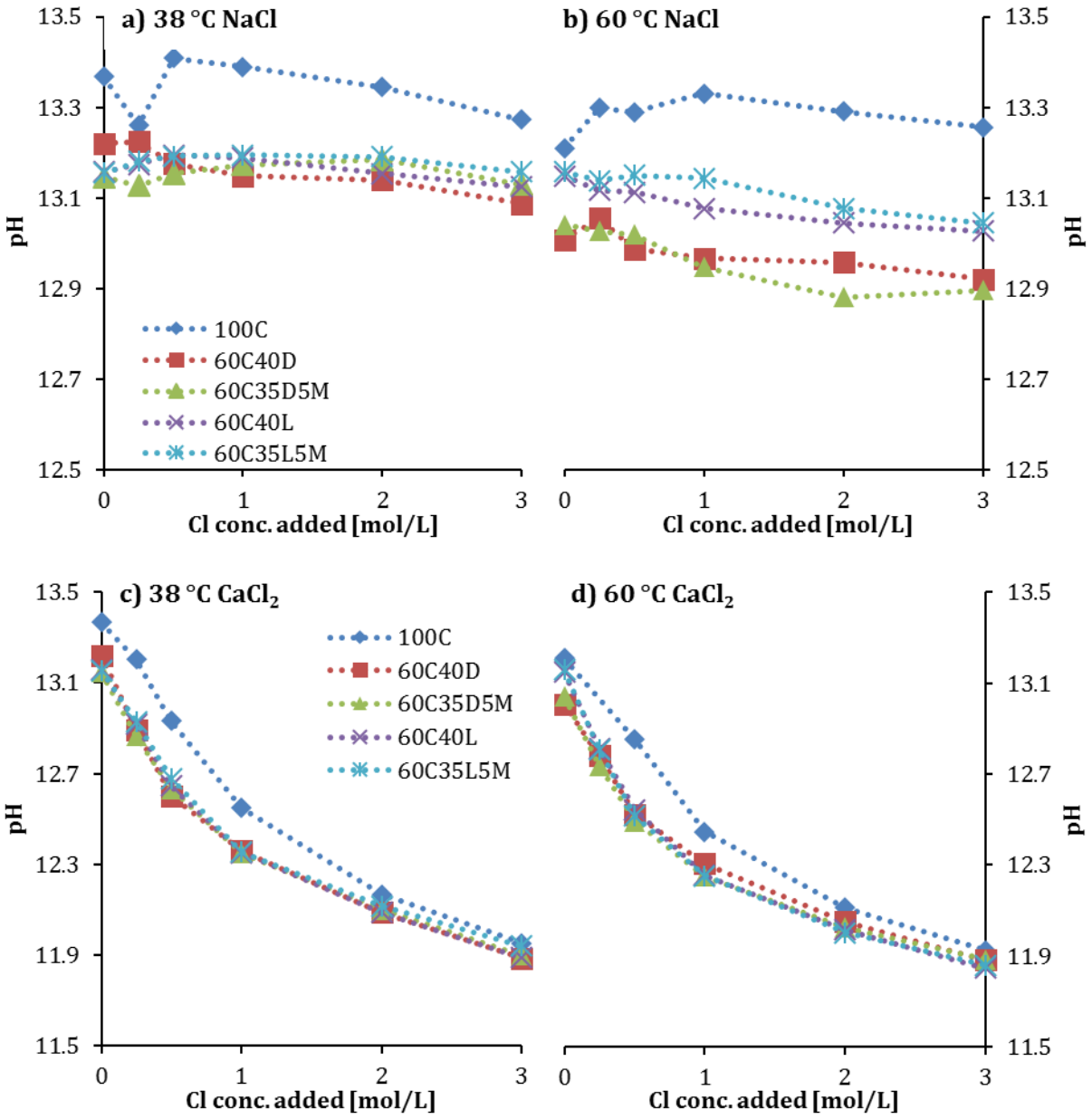

Figure 5: pH measurements of the supernatant of the various binder compositions cured at 38 °C or 60 °C and exposed to various concentrations of NaCl or $CaCl_2$. The measurements were performed at 20 °C. The points at 0 mol/L refer to the pH measurements of the reference samples exposed to deionized water.

1003

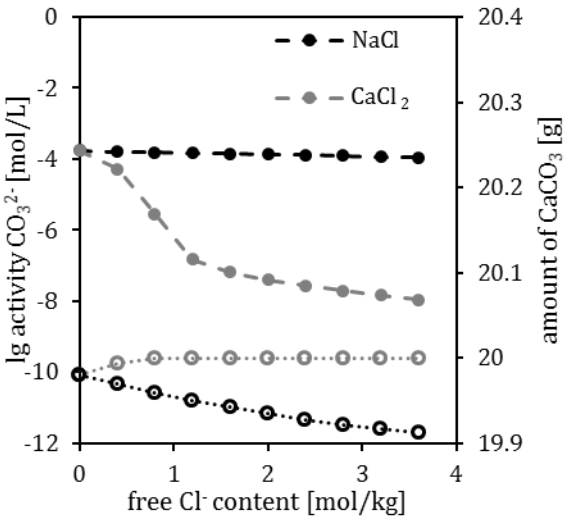

Figure 6: Results of the thermodynamic modelling of the activity of CO_3^{2-} ions (*filled icons, dashed lines, plotted as* log_{10}) in the pore solution and the amount of $CaCO_3$ present in the system (*hollow icons, dotted lines*) with increasing additions of NaCl or $CaCl_2$.

1004

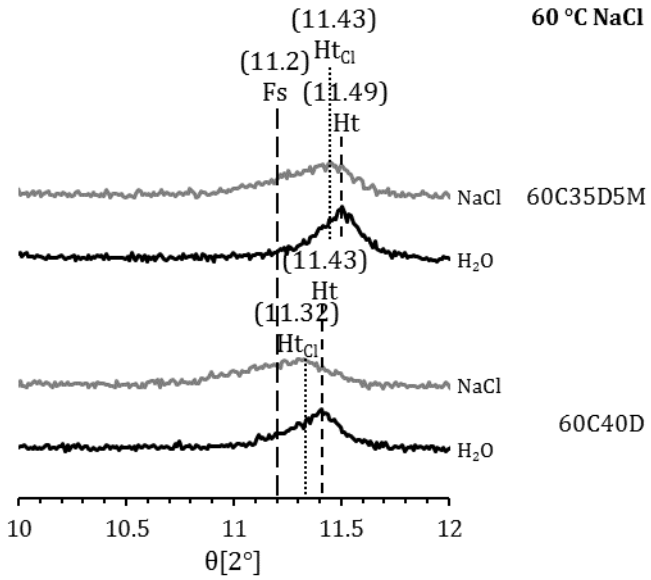

Figure 7: Zoomed in XRD patterns between 10 and 12 °2θ of the samples 60C40D and 60C35D5M cured at 60 °C that were exposed to NaCl compared with their reference samples exposed to deionized water.

1005

1006

1007

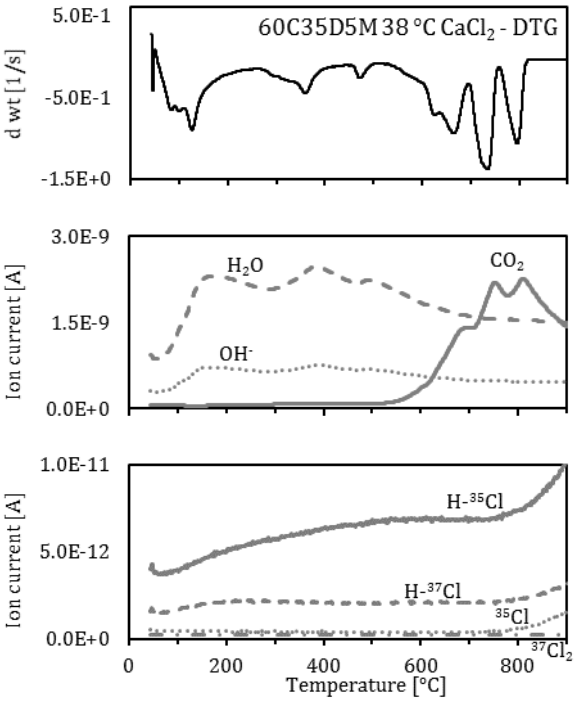

Figure 8: Mass spectra of the various components released during TGA-MS investigations of sample 60C35D5M cured at 38 °C and exposed to $CaCl_2$. Note the different scaling on the y-axes.

1008

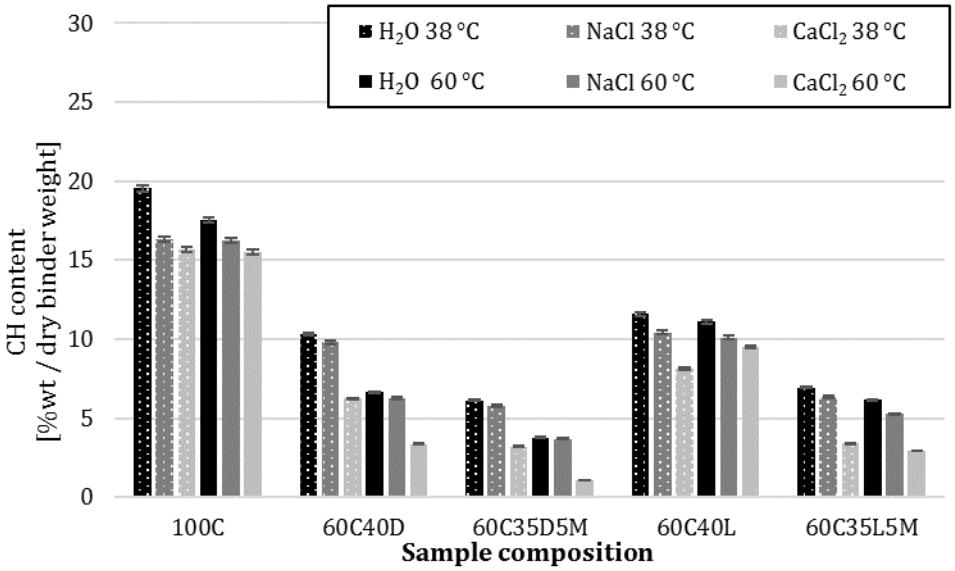

Figure 9: Portlandite content normalized to the dry binder weight for the various samples cured at 38 °C or 60 °C that were exposed to H_2O, NaCl or $CaCl_2$.

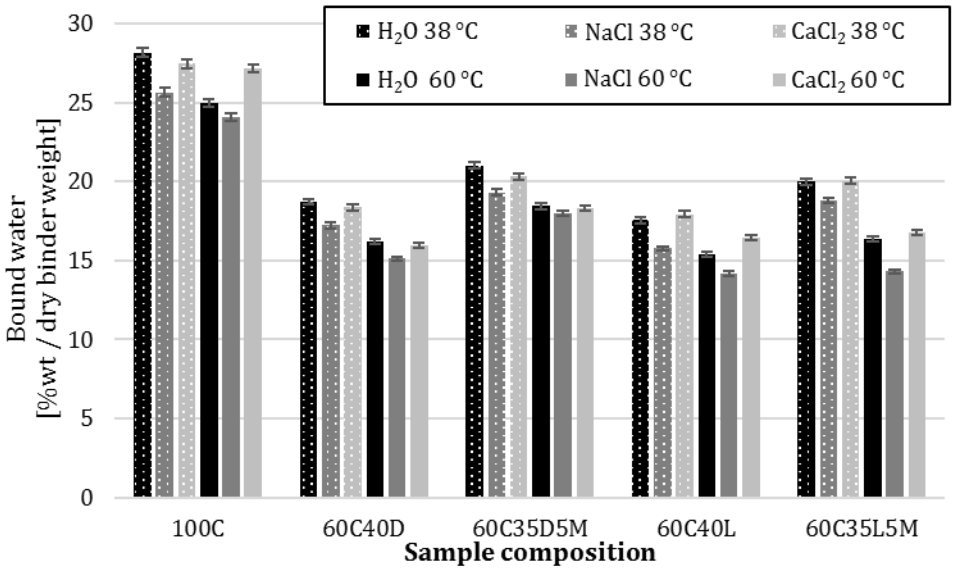

Figure 10: Bound water content normalized to the dry binder weight for the various samples cured at 38 °C or 60 °C that were exposed to H_2O, NaCl or $CaCl_2$.

1009

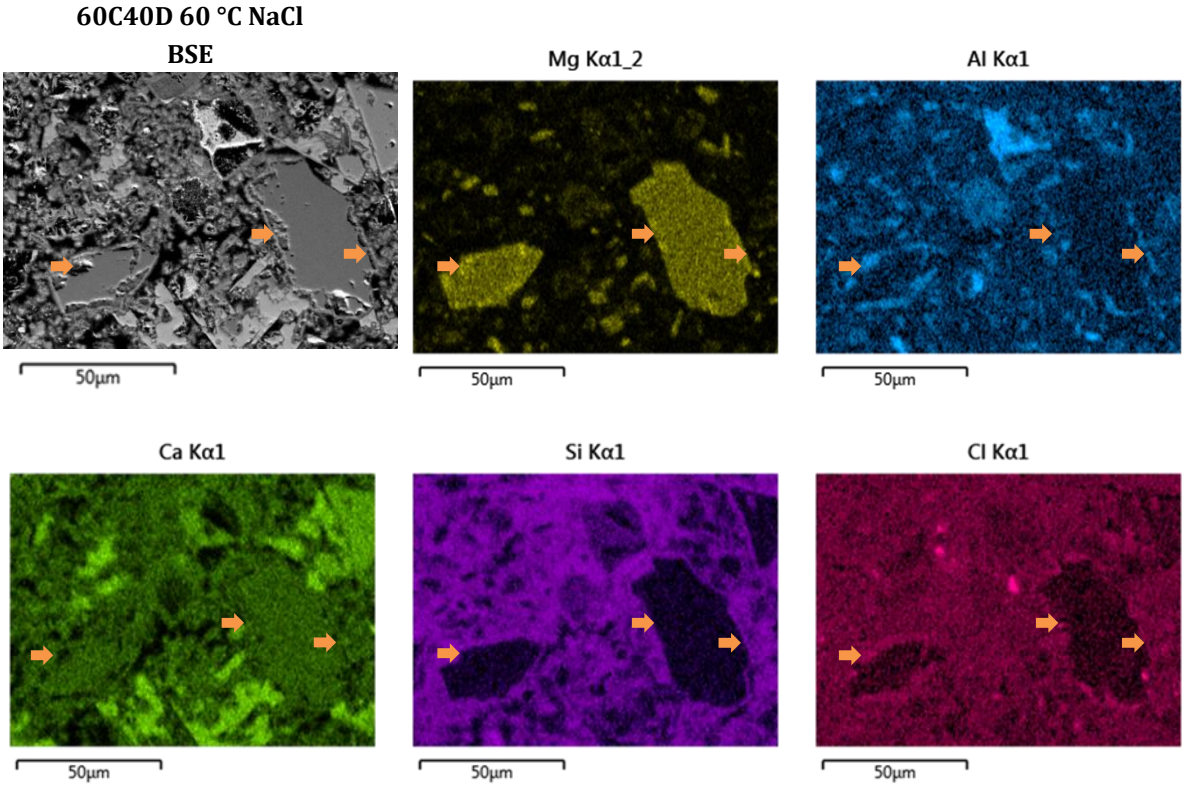

Figure 11: BSE image and elemental maps of magnesium, aluminium, calcium, silicon and chlorine for sample 60C40D cured at 60 °C and exposed to a 2 mol/L NaCl solution.

1010

1011

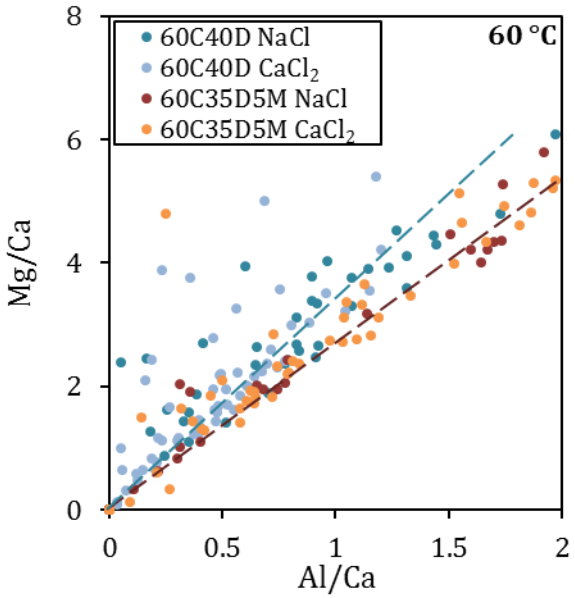

Figure 12: Mg/Ca ratio over the Al/Ca ratio for the point analyses of the reaction rims around the dolomite grains in samples 60C40D and 60C35D5M, which were cured at 60 °C and exposed to NaCl or $CaCl_2$.

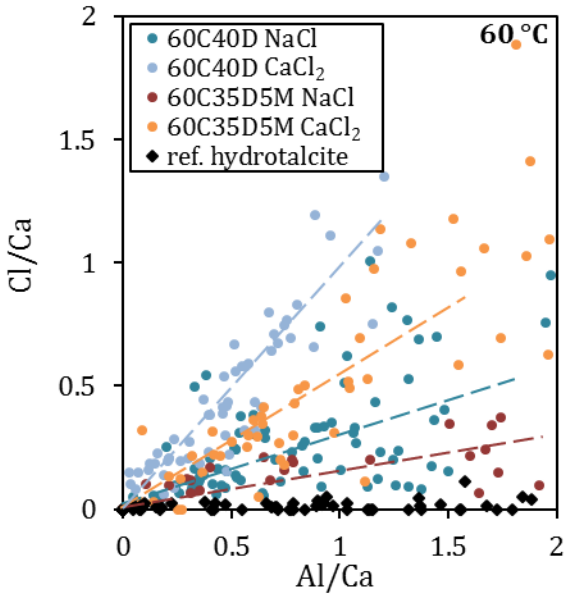

Figure 13: Cl/Ca ratio over the Al/Ca ratio for the point analyses of the reaction rims around the dolomite grains in samples 60C40D and 60C35D5M, which were cured at 60 °C and exposed to NaCl or $CaCl_2$. In addition, the results for the point analyses in such reaction rims from a previous study [10] are shown as a reference for not-exposed samples.

1012

1013

1014

1015

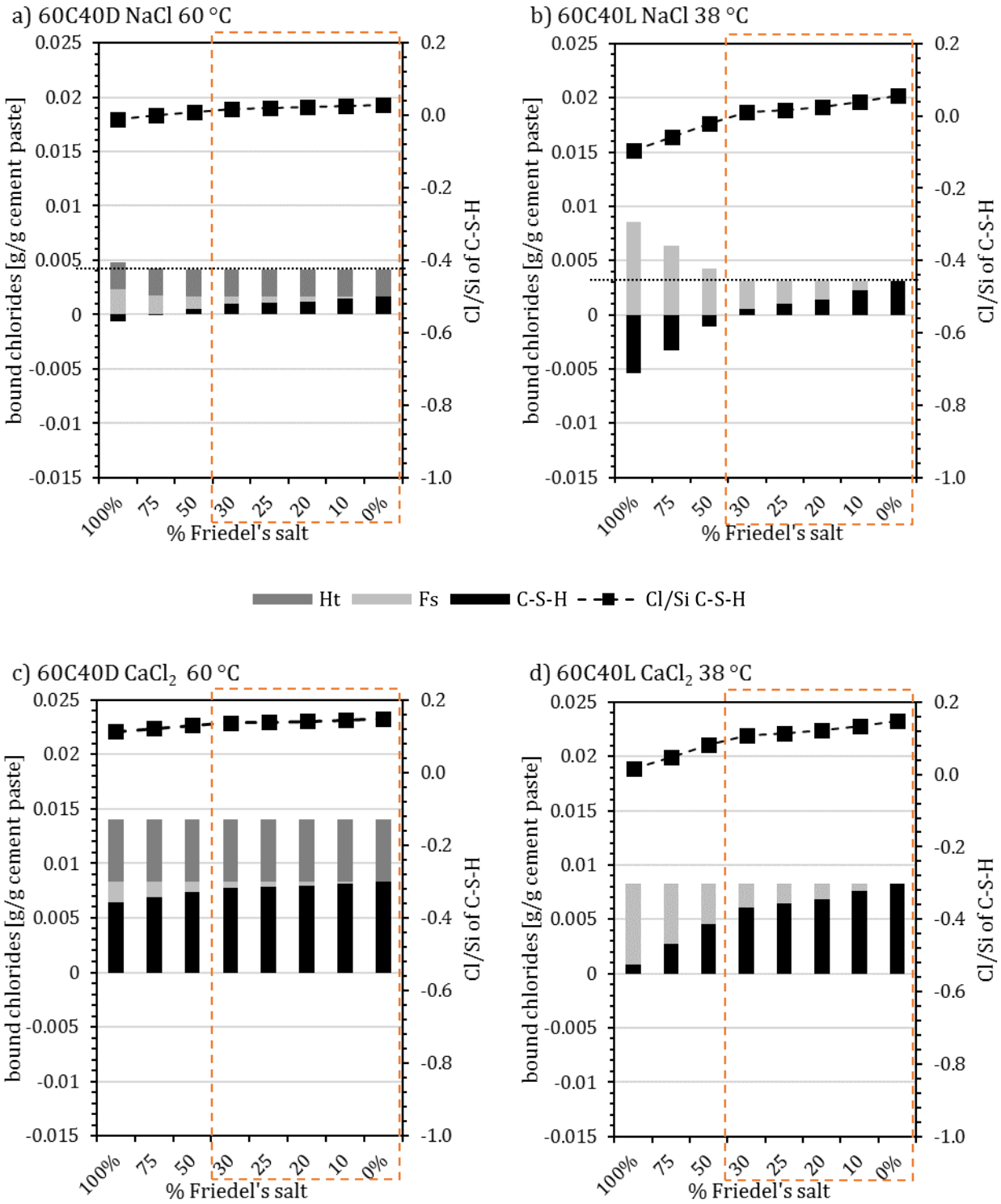

Figure 14: Calculated Cl/Si ratio of the C-S-H and amount of chloride bound in C-S-H, Friedel's salt, and hydrotalcite calculated for the samples 60C40D (60 °C) and 60C40L (38 °C) exposed to NaCl or $CaCl_2$ depending on the distribution of the aluminium between Friedel's salt and monocarbonate. The dotted lines in a) and b) indicate the amount of bound chlorides determined with potentiometric titration (see Figure 3).

1016

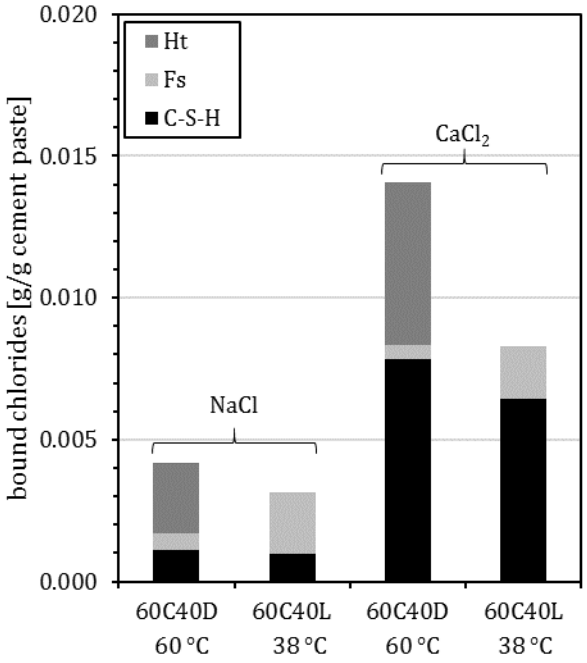

Figure 15: Amount of chloride bound in C-S-H, Friedel's salt, and hydrotalcite calculated for the samples 60C40D (60 °C) and 60C40L (38 °C) exposed to NaCl or $CaCl_2$, when 25% of the aluminium available for the formation of AFm phases is distributed to Friedel's salt (and 75% to monocarbonate).

8 Appendix

8.1 Hydrate phase assemblage in the exposed samples

8.1.1 XRD

Figure A1 a), b) and Figure A2 a), b) show the XRD patterns between 8 and 13 °2θ for the samples containing dolomite exposed to NaCl or $CaCl_2$ and their reference samples exposed to deionized water. The peak positions of ettringite (Et – 9.1 °2θ), monosulphate (Ms – 9.9 °2θ), Friedel's salt (Fs – 11.2 °2θ), monocarbonate (Mc – 11.7 °2θ), hydrotalcite (Ht – approx. 11.4 °2θ) and the chloride-containing hydrotalcite (Ht_{Cl} – approx. 11.1–11.3 °2θ) are also indicated.

Whether exposed to NaCl or $CaCl_2$, the samples show very similar qualitative phase assemblages, so they are described together in the following, with differences highlighted.

Sample 60C40D shows a qualitatively similar phase assemblage whether cured at 38 °C or 60 °C. In both cases, hydrotalcite was observed in the reference samples exposed to water and, with chloride exposure, this peak shifted to lower angles. This shift was reported to be due to the formation of a chloride-containing hydrotalcite-like phase [13]. The peaks of hydrotalcite and chloride-containing hydrotalcite were both higher in samples cured at 60 °C than in samples cured at 38 °C. In samples with metakaolin added in combination with dolomite (60C35D5M), monocarbonate was observed as well as a small peak of hydrotalcite in the reference samples cured at 38 °C. In the samples exposed to chloride solutions, the monocarbonate transformed to Friedel's salt. The Friedel's salt and chloride-containing hydrotalcite peaks overlap, so no conclusion on the presence of small amounts of chloride-containing hydrotalcite can be drawn for this sample with XRD. Cured at 60 °C, sample 60C35D5M showed no peaks of monocarbonate or Friedel's salt. As with sample 60C40D only hydrotalcite, in the case of water exposure, or the chloride-containing hydrotalcite, in the case of chloride exposure, were observed. The ettringite observed in the reference samples seemed to be reduced by the exposure to chloride solutions or to disappear completely. The only exception was sample 60C35D5M, which also showed an increase in the ettringite peak when originally cured at 60 °C as opposed to 38 °C. For the compositions for which ettringite could be observed when exposed to deionized water, a monosulphate-14H peak was observed instead of ettringite when exposed to $CaCl_2$.

Figure A3 a), b) and Figure A4 a), b) show the XRD patterns of the samples containing limestone exposed to NaCl or $CaCl_2$ and their reference samples exposed to deionized water. In samples containing limestone cured at 38 °C, the AFm phase observed in water-exposed samples was monocarbonate, while in chloride-exposed samples the AFm phase was mainly Friedel's salt. No

monocarbonate peak was observed in any of the samples cured at 60 °C, and only a small hump of Friedel's salt was detected in sample 60C35L5M (60 °C) exposed to NaCl. As with the samples containing dolomite, the ettringite peak seemed to be reduced by exposure to chloride solutions and a monosulphate-14H peak was observed in the samples exposed to $CaCl_2$. Sample 60C40L showed an especially high ettringite peak in the samples cured at 60 °C compared to 38 °C.

8.1.2 TGA

The TGA results for the samples exposed to NaCl or $CaCl_2$ were generally quite similar so they are described together in the following, with differences highlighted.

Figure A1 c), d) and Figure A2 c), d) show the DTG curves of the samples containing dolomite exposed to NaCl or $CaCl_2$ and their reference samples, which were exposed to deionized water. Samples containing dolomite and cured at 38 °C showed a clear ettringite peak in samples exposed to deionized water, and to a lesser degree in the samples exposed to NaCl or $CaCl_2$. The samples containing a combination of metakaolin and dolomite showed a clear peak of monocarbonate where exposed to water, and of Friedel's salt were exposed to chloride solution. Neither monocarbonate nor Friedel's salt were observed with TGA in samples containing dolomite that did not contain metakaolin, indicating that most of the aluminium is bound in the hydrotalcite. The only exception to this was sample 60C40D exposed to $CaCl_2$, which showed a small peak of Friedel's salt. Due to the overlap of the second peak of Friedel's salt (approx. 370 °C) with the decomposition temperature of chloride-containing hydrotalcite, the appearance of the first peak (approx. 150 °C) was used to identify Friedel's salt in the sample. This first Friedel's salt peak was more pronounced in samples exposed to $CaCl_2$ than in samples exposed to NaCl. This observation confirms the findings of Shi et al., who reported additional formation of Friedel's salt in samples exposed to $CaCl_2$ due to the increased availability of calcium ions [3]. Hydrotalcite also showed two peaks in TGA, the first of which (approx. 220 °C) was significantly reduced or completely vanished in the samples exposed to chloride solutions instead of deionized water. The second peak of hydrotalcite (approx. 400 °C) shifted to lower temperatures (approx. 370 °C) in samples exposed to chloride solutions. On this peak, the shoulder of a Friedel's salt peak at even lower temperatures was observed in samples that also showed the first Friedel's salt peak. The portlandite peak seemed little affected by exposure to NaCl, but it was significantly lower in samples containing metakaolin or exposed to $CaCl_2$.

In samples containing dolomite cured at 60 °C, the ettringite peak was significantly lower compared to 38 °C, especially in samples containing no metakaolin. AFm phases like monocarbonate or Friedel's salt were no longer observed. Only sample 60C40D cured at 60 °C and

exposed to $CaCl_2$ showed a peak of monocarbonate. The peaks related to hydrotalcite or chloride-containing hydrotalcite were higher than in samples cured at 38 °C. In both cases, the chloride-containing hydrotalcite could be distinguished by the significantly lower or missing first peak and the shift to lower temperatures of the second peak compared to the normal hydrotalcite. This was observed in all samples except sample 60C35D5M cured at 60 °C exposed to NaCl, which showed only a slight decrease in the first peak and no shift for the second peak. In samples cured at 60 °C, the portlandite content seemed lower in samples with NaCl exposure, metakaolin addition and especially with $CaCl_2$ exposure.

The DTG curves for the samples containing limestone exposed to NaCl or $CaCl_2$ and their reference samples exposed to deionized water are shown in Figure A3 c), d) and Figure A4 c), d). Like the samples containing dolomite, the samples containing limestone cured at 38 °C, showed a clear ettringite peak at low temperatures that seemed to decrease when exposed to NaCl or $CaCl_2$ compared to the references exposed to water. In the latter case, there was a clear peak of monocarbonate, which was even greater for samples containing metakaolin. In samples exposed to $CaCl_2$, a clear Friedel's salt peak was observed instead of monocarbonate. This was also the case in samples exposed to NaCl, but it was less clear and combined with a monocarbonate peak. The reference samples containing limestone exposed to deionized water also showed very small peaks in the temperature region of hydrotalcite. This weight loss might be caused by hydrotalcite formed due to the large amount of magnesium present in the cement (Table 1). In the samples containing limestone exposed to NaCl or $CaCl_2$, a clear peak of Friedel's salt and what was probably a small peak of chloride-containing hydrotalcite was observed. As with the samples containing dolomite, the portlandite peak was only affected by the presence of metakaolin or the exposure to $CaCl_2$.

In samples containing limestone cured at 60 °C, the ettringite peak was again lower than in those cured at 38 °C, though the decrease was not as great as in the samples containing dolomite. No AFm phases were observed with TGA, except for a small peak of Friedel's salt in sample 60C35L5M exposed to $CaCl_2$. As in the samples containing dolomite, the peaks related to hydrotalcite were higher in samples cured at 60 °C than in samples cured at 38 °C. The Friedel's salt peak in the chloride-exposed samples showed a clear asymmetry or a double peak, indicating also an increase in the amount of chloride-containing hydrotalcite. The portlandite peak was reduced by both chloride exposures, but especially by exposure to $CaCl_2$, and in samples with metakaolin.

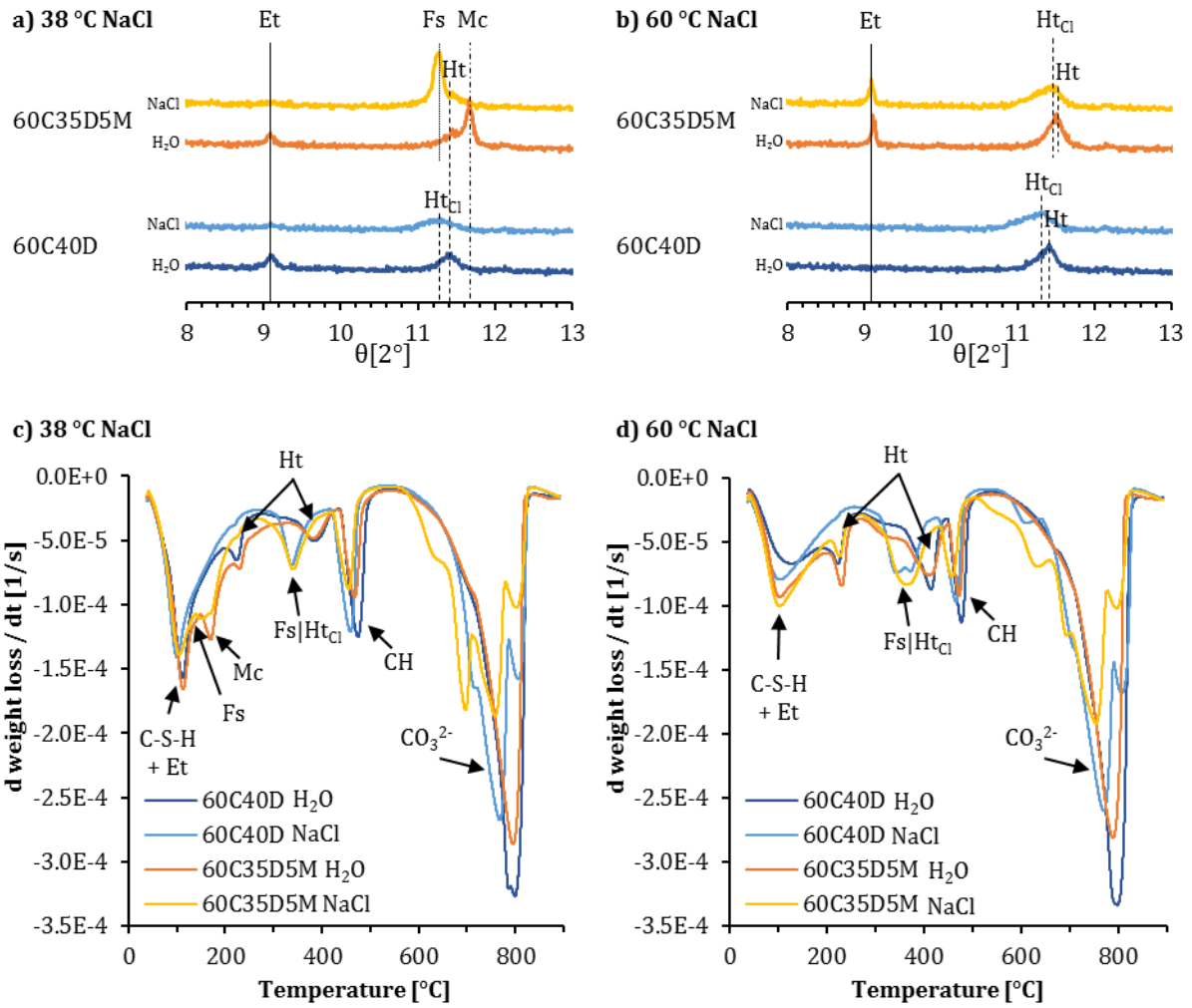

Figure A1: Phase assemblage of the samples containing dolomite cured at 38 °C or 60 °C that were exposed to 2 mol/L NaCl compared with their reference samples exposed to deionized water. a) and b) show the XRD patterns of these samples between 8 and 13 °2θ, and c) and d) show the DTG curves of these samples from 40–900 °C.

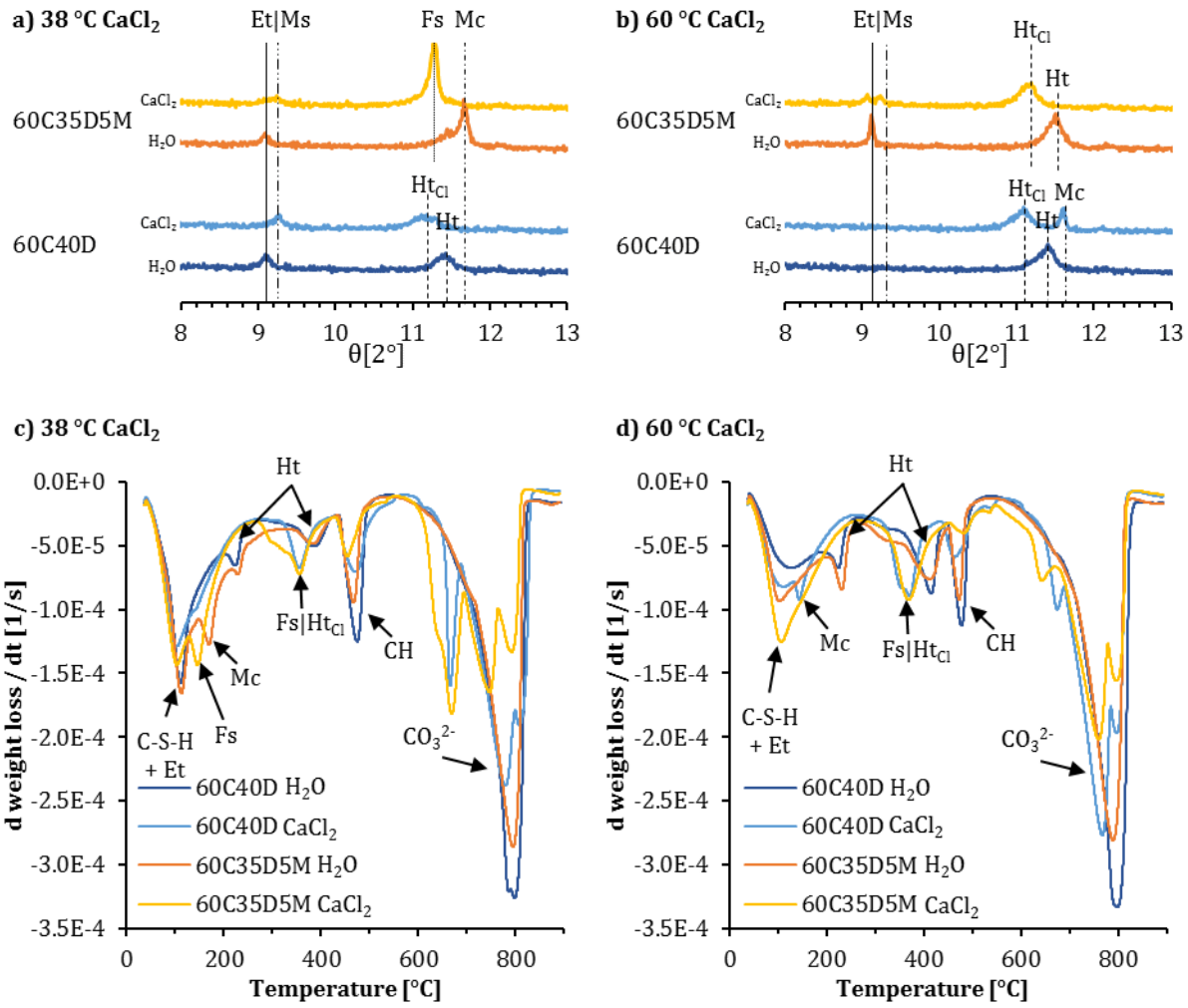

Figure A2: Phase assemblage of the samples containing dolomite cured at 38 °C or 60 °C that were exposed to 2 mol/L $CaCl_2$ compared with their reference samples exposed to deionized water. a) and b) show the XRD patterns of these samples between 8 and 13 °2θ, c) and d) show the DTG curves of these samples from 40–900 °C.

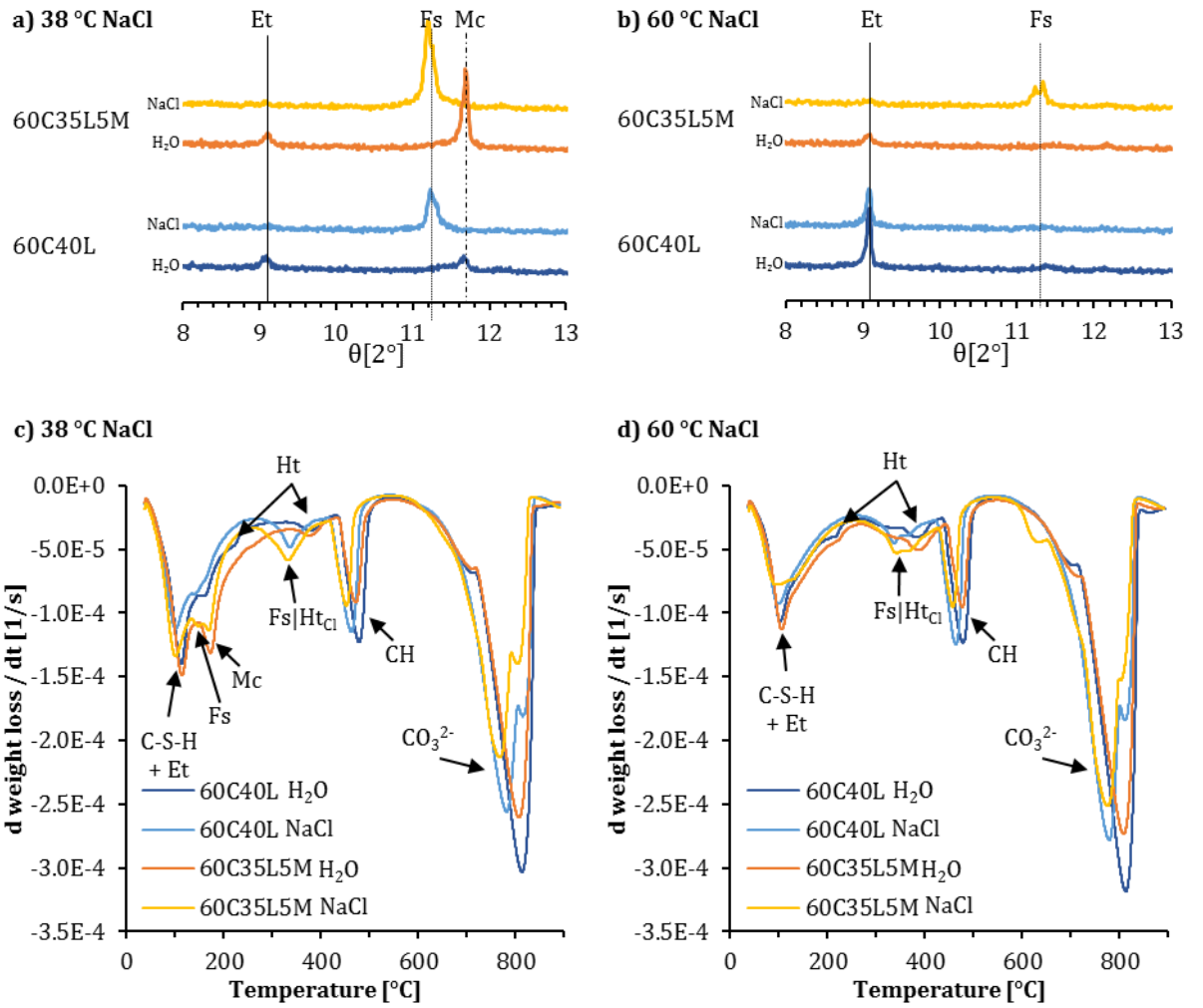

Figure A3: Phase assemblage of the samples containing limestone cured at 38 °C or 60 °C that were exposed to 2 mol/L NaCl compared with their reference samples exposed to deionized water. a) and b) show the XRD patterns of these samples between 8 and 13 °2θ, c) and d) show the DTG curves of these samples from 40–900 °C.

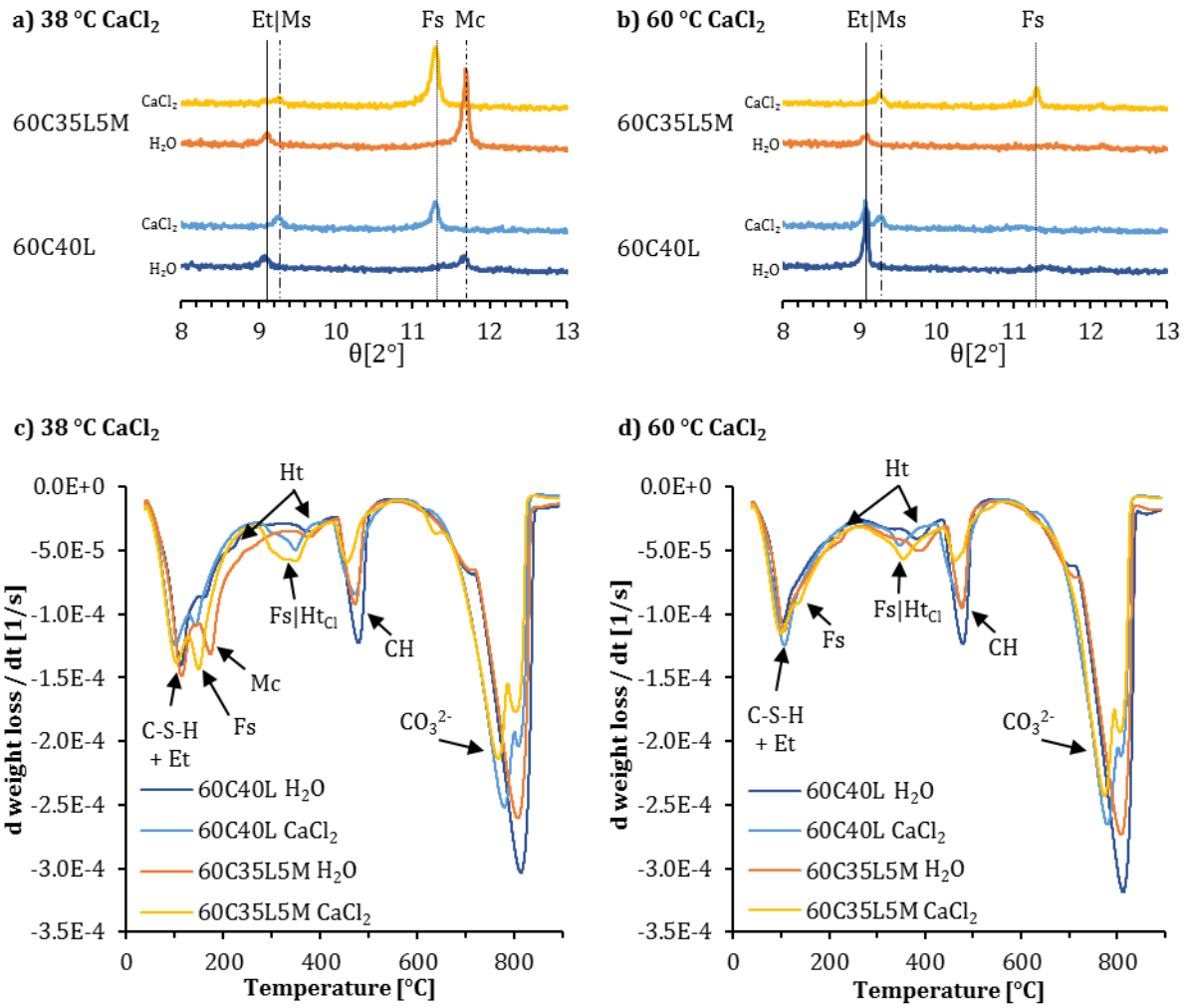

Figure A4: Phase assemblage of the samples containing limestone cured at 38 °C or 60 °C that were exposed to 2 mol/L $CaCl_2$ compared with their reference samples exposed to deionized water. a) and b) show the XRD patterns of these samples between 8 and 13 °2θ, c) and d) show the DTG curves of these samples from 40–900 °C.

1132